HYBRIDIZED ENZYMATIC-CHEMOCATALYTIC CONVERSION OF CELLULOSIC BIOMASS TOWARDS SUSTAINABLE BIOENERGY

A THESIS REPORT

SUBMITTED TO THE FACULTY OF ENGINEERING & TECHNOLOGY

JADAVPUR UNIVERSITY

IN PARTIAL FULFILMENT OF THE REQUIREMENTS FOR THE AWARD OF THE DEGREE OF

MASTER OF ENGINEERING

IN BIO-PROPROCESS ENGINEERING

By

DIPA POREL

Examination Roll No M4BPE24002

Registration No 131671 of 2015-2016

Under the Guidance of

PROF. RAJAT CHAKRABORTY

DEPARTMENT OF CHEMICAL ENGINEERING

FACULTY OF ENGINEERING AND TECHGNOLOGY

JADAVPUR UNIVERSITY

Kolkata-700032

Session: 2022-2024

Declaration of Originality and Compliance of Academic Ethics

I hereby declare that this thesis contains literature survey and original research work by the undersigned candidate, as part of his Master of Chemical Engineering in Bio-Process Engineering faculty of Engineering and Technology, Jadavpur University, Session: 2022-2024 studies. All information in this document have been obtained and presented in accordance with academic rules and ethical conduct**.**

I also declare that, as required by these rules and conduct, I have fully cited and referenced all material and results that are not original to this work.

Name: Dipa Porel

Roll Number: M4BPE24002

Thesis Title: HYBRIDIZED ENZYMATIC-CHEMOCATALYTIC CONVERSION OF CELLULOSIC BIOMASS TOWARDS SUSTAINABLE BIOENERGY

Signature with date:

……

(DIPA POREL)

Date: ……

CERTIFICATE OF RECOMMENDATION

I hereby recommend that the thesis prepared under my supervision by Rupam Mandal, entitled**, "HYBRIDIZED ENZYMATIC-CHEMOCATALYTIC CONVERSION OF CELLULOSIC BIOMASS TOWARDS SUSTAINABLE BIOENERGY"** be accepted in partial fulfilment of the requirements for awarding the degree of Master of Bio-Process Engineering under Department of Chemical Engineering of Jadavpur University.

……..

PROF. RAJAT CHAKRABORTY

Thesis Advisor

Dept. of Chemical Engineering

Jadavpur University

Kolkata

……..

Professor & Head

Dept. of Chemical Engineering

Jadavpur University

Kolkata

…….

Dean

Faculty of Engineering and Technology

Jadavpur University

Kolkata

Certificate of Approval

The foregoing thesis, entitled as is hereby approved by the committee of final examination for evaluation of thesis as a creditable study of an engineering subject carried out and presented by **Ms. Dipa Porel (Examination Roll No.- M4BPE24002);** in a manner satisfactory to warrant its acceptance as a perquisite to the degree of Master of Chemical Engineering. It is understood that by this approval, the undersigned do not necessarily endorse or approve any statement made, opinion expressed or conclusion drawn therein, but approve the thesis only for the purpose for which it is submitted.

Committee of final examination for evaluation of thesis.

……

…….

DEDICATED

TO MY BELOVED PARENTS

WHO ARE MY

SPIRITUAL GUIDE

ACKNOWLEDGEMENT

During my M.E. programme I have been facing a lot of ups and downs but nothing could resist my quest. Therefore, I meet the result at the end and it is the time to express my gratitude to those who helped me to make this journey memorable.

First of all, I would like to express my sincere gratitude to my supervisor Prof. Rajat Chakraborty Department of Chemical Engineering, Jadavpur University, Kolkata, India for his never-ending support in my M.E journey. I would be always thankful for his guidance, motivation and helpful attitude. His knowledge and experience guided me a lot during the M.E program and to complete my thesis work also. He is always there with his support and willingness to make my work profound and effective. We spent long hours together to get a fruitful result. It is my honour that he took faith on me and encouraged me to walk in such a tough way to reach my goal. It's beyond my imagination that any advisor can be better than him for my M.E journey.

I convey my special thanks to my PhD senior Ms. Sohini Roy Choudhury for her eminent help & guidance throughout my entire M.E course. Words are not enough to express my gratitude for her endless co-operation.

I would also like to thank my friend Mr. Rupam Mandal, PhD scholar of Department of Mechanical Engineering, Jadavpur University for his sincere help with some characterization tests, without which my research would take more time.

My heartiest gratitude to my family members for their unflagging love and support throughout my life. I am highly grateful to my parents for their blessing, love, encouragement and support in every aspect of my life.

Lastly, I acknowledge that it is not possible to list all those who have contributed to this thesis, but their views and tips have been invaluable and are greatly appreciated.

- - - - - - - - - - - - - - -

(Dipa Porel)

Date:

LIST OF FIGURES

Figure No.	Figure Name	Page No.
1	Ethanol demand from 2013-2024	5
2	WBP components	7
3	Flowchart of various pretreatment processes for lignocellulosic biomass	8
4	Hot air oven	29
5	Image of IRSBB	30
6	WBP before pretreatment	31
7	Pretreated WBP	31
8	Hot water washing of PWBP	31
9	Isolation of lignin	32
10	Model of CIIVBR	33
11	Ultrasonic Homogenizer	34
12	Magnetic property of CIMPI in presence of magnet	35
13	FS in presence of DNS	35
14	Standard curve of glucose at 540 nm	37
15	a) batch fermentation using S. cerevisiae, b) bio-ethanol purification using distillation setup	38
16	SEM instrument	40
17	TGA instrument	41
18	FTIR instrument	42
19	XRD instrument	43
20	BET instrument	44
21	Example of a chromatogram	45
22	LCA boundary system	51
23	DNS samples using L9TED	54
24	HPLC of saccharified substance from PWBP using CIMPI chemo-biocatalyst under CIIVBR	57

25	Main effect plot for SN ratio	59
26	XRD pattern of PWBPSS, PWBP, WBP	59
27	SEM images of iron oxide particles at a) 10000x and b) 50000x magnification	60
28	SEM images of CIMPI under a) 10000x and b) 50000x magnification	61
29	Elemental mapping of Fe_3O_4	62
30	EDAX of Fe_3O_4 particle	62
31	Elemental mapping of CIMPI	63
32	EDAX of CIMPI	63
33	(a)X-ray diffraction pattern; (b) TGA; (c) FTIR; (d) UV-vis spectrum& Tauc Plot (band gap) of CIMPI	66
34	a) Surface area isotherm**,** b) BJH plot and c) Adsorption isotherm depicting BET of CIMPI	67
35	PL spectra of CIMPI	68
36	CIMPI reusability cycles	69
37	Plausible reaction mechanism of CIMPI chemo-biocatalyst	70
38	Variation in FS concentration with time during saccharification of PWBP employing CIIVBR and CBR using CIMPI and free cellulase enzyme	72
39	Bio-ethanol production (g/l) and fermentable sugar conversion (%) in every 12h	73
40	(a) Relative percentage contribution of different sub processes covering the boundary system;(b) Comparative environmental impact analysis of recycled CIMPI over fresh CIMPI; (c) Comparative environmental impacts of CIIVBR, CBR, and FS to bio-ethanol	75
41	Main effects plot for SN ratio	77
42	XRD of CIPSn	78
43	FTIR of CIPSn	79
44	TGA of CIPSn	79

LIST OF TABLES

Table No.	Table Name	Page No.
1.	Compositional analysis of WBP and PWBP	30
2.	Independent process variables for saccharification of PWBP with CIMPI	36
3.	LCI database for 1 Kg PWBP preparation	48
4.	LCI database for 1 Kg of optimal CIMPI preparation	48
5.	LCI database for 1 Kg FS production in CIIVBR	49
6.	LCI database for 1 Kg FS production in CBR	50
7.	LCI database for 1 Kg Bio-ethanol production	50
8.	Compositional analysis of WBP and PWBP	52
9.	Independent process variables for saccharification of PL with CIPSn	53
10.	Representing 9 experimental runs as per L9TED	58
11.	Representing 9 experimental runs as per L9TED using CIPSn	76

CONTENTS

CONTENT	PAGE NO.
1. Abstract	1-2
2. Introduction	3-14
3. Literature Review	15-22
4. Research Gaps	23-24
5. Aims & Objectives	25-26
6. Materials & Methods	27-55
i. Materials for production of Bio-ethanol from WBP	28
ii. Materials for production of FS from PL	28
Methods for production of Bio-ethanol from WBP	
i. Physical pretreatment of waste banana pseudo-stem	29
ii. AFEX Pre-treatment	29
iii. Chemical pretreatment of waste banana pseudo-stem	
iv. Cellulase immobilization on magnetic photo-active iron particles	30
v. Saccharification of pretreated waste banana pseudostem (PWBP) with free cellulase enzyme	32
vi. Saccharification of PWBP with CIMPI	33
vii. Experimental layout and process optimization using Taguchi design	33-35
viii. UV-vis spectroscopy analyses of pretreated waste banana pseudostem saccharified substance (PWBPSS)	35-36
ix. HPLC analyses of PWBPSS	36-37
x. Preparation of yeast mixture and bio-ethanol production from FS of PWBP	37
xi. Characterization tests of the prepared CIMPI	37-39
xii. Life cycle analysis (LCA) study	
Methods for production of FS from PL	39-47
i. Physical pretreatment of pineapple leaves	47-51

ii.	Chemical pretreatment of waste banana pseudo-stem	52
iii.	Cellulase immobilization on magnetic photo-active iron particles	52
iv.	Saccharification of PL with CIPSn	52
v.	Experimental process optimization using Taguchi design	53
vi.	UV-vis spectroscopy analyses of pretreated PL saccharified substance (PPLSS)	53
vii.	Characterization tests of the prepared CIPSn	54
		55
7.	**Result & Discussion**	56-80
Results and discussion for WBP to Bio-ethanol conversion using CIMPI		
i.	WBP and PWBP composition analysis	57
ii.	FS yield analysis via UV Spectroscopy	57
iii.	FS yield analysis via HPLC	57
iv.	Optimization of FS yield	58
v.	Characterization of WBP, PWBP and PWBPSS	59
vi.	Characterization of the prepared optimal chemo-biocatalyst (CIMPI)	60-68
vii.	CIMPI Reusability Analysis	68-69
viii.	CIMPI chemo-biocatalyst mechanism	69-70
ix.	Energy efficiency of CIIVBR	70-72
x.	Analysis of bio-ethanol yield	72-73
xi.	LCA analysis	73-75
Results and discussion for PL to FS conversion using CIPSn		
i.	PL and PPL composition analysis	75-76
ii.	FS yield analysis via UV Spectroscopy	76
iii.	Optimization of FS yield	76-77
iv.	Characterization of the prepared optimal chemo-biocatalyst	77-79
8.	**Conclusion & Future scope**	80-82
9.	**References**	83-92

CHAPTER 1

ABSTRACT

1. ABSTRACT

An environmentally sustainable cellulase immobilized magnetic-photoactive iron (CIMPI) chemo-biocatalyst was synthesized at varying Fe_3O_4 concentrations for the valorization of waste banana pseudostem (WBP) into fermentable sugar (FS) employing an energy-efficient carbon-infrared irradiated (100 W, 750–1400 nm) vibrating batch reactor (CIIVBR). To improve the efficiency of WBP pretreatment for delignification, peracetic acid treatment was conducted in the CIIVBR. The pretreated WBP (PWBP) was saccharified in the CIIVBR using CIMPI as per L9 Taguchi experimental design (L9TED) to maximize the fermentable sugar yield (73.40%) corresponding to 60 min batch time, 50°C CIIVBR temperature,3:1 (w/w) water: PWBP, and 3.5 wt.%. CIMPI concentration. The optimal CIMPI was characterized using XRD, SEM, EDAX, TGA, FTIR, BET, UV-Vis, and PL analyses. CIMPI exhibited a bandgap of 3.01 eV, confirming its photoactive nature.CIMPI could be recovered conveniently due to its magnetic properties and even after recycling for 6^{th} cycle, it could retain upto71% of its initial activity. The CIIVBR could save 80% energy compared to the conventional batch reactor (CBR)at the optimal condition, underscoring the superior energy-efficiency of the novel CIIVBR. The optimally produced FS, was subsequently converted into bio-ethanol using dry yeast viz. *Saccharomyces cerevisiae* yielding a maximum of 24.2g/l. Life cycle assessment (LCA) of the overall WBP photoactive-chemo-bioconversion process substantiated remarkable reduction in the Global Warming Potential (GWP100) by 37.5%, Acidification Potential (AcidP) by 18.36%, and Water Depletion Potential (WDP) by 27.27% compared to conventional process.

Another novel chemo-biocatalyst, cellulase immobilized photoactive tin (CIPSn), was synthesized via the calcination of tin chloride to tin oxide and following the similar method. Characterization techniques including X-ray diffraction (XRD), thermogravimetric analysis (TGA), and Fourier-transform infrared spectroscopy (FTIR) were employed to analyze the structural and chemical properties of the CIPSn catalyst. Subsequently, pineapple leaves underwent pretreatment, and the saccharification process was conducted using CIPSn. Optimization of the saccharification process was achieved using L9 Taguchi experimental design (L9TED). The results indicated that a maximum fermentable sugar (FS) yield of 56.7% could be obtained using the optimized conditions. Additionally, the formation of other chemicals was observed during the saccharification process. This study presents a promising approach for the efficient conversion of biomass into fermentable sugars using a novel immobilized chemo-biocatalyst, CIPSn.

CHAPTER 2

INTRODUCTION

2. Introduction

Biofuel is a type of fuel that is derived from renewable biological sources, such as plants, algae, or organic waste. Unlike traditional fossil fuels that come from finite resources like coal or oil, biofuels are considered more sustainable because the plants used to produce them can be grown and harvested on a continuous basis. Common types of biofuels include ethanol, which is often made from crops like corn or sugarcane, and biodiesel, which is typically produced from vegetable oils or animal fats. The use of biofuels is often promoted as a way to reduce dependence on non-renewable energy sources and decrease the overall carbon footprint associated with energy production and consumption (Bindra et al.,2017, Hassan et al.,2013). Biofuels are derived from organic materials such as plants, algae, and waste, which can be replenished through cultivation or natural processes. Unlike finite fossil fuels, biofuels offer a renewable and sustainable source of energy (Kour et al.,2019). When biofuels are burned, they release carbon dioxide (CO_2) into the atmosphere. However, the plants used to produce biofuels absorb CO_2 during their growth, creating a closed carbon cycle (Searchinger et al.,2010). This contrasts with fossil fuels, where burning releases carbon that has been sequestered underground for millions of years, contributing to a net increase in atmospheric CO_2 levels. Therefore, biofuels can help mitigate the impact of greenhouse gas emissions on climate change (Bessou et al.,2011). Biofuels can contribute to energy security by diversifying the sources of energy. By reducing reliance on imported fossil fuels, countries can enhance their energy independence and resilience to geopolitical uncertainties related to oil and gas (Meidan et al.,2023).

Bioethanol is compatible with existing infrastructure for gasoline. It can be blended with gasoline in various proportions, allowing for a gradual transition and easier integration into the existing transportation system. This adaptability makes it a more practical and accessible alternative compared to some other biofuels (Teferra,2022). When petrol is blended with ethanol, its performance improves because the former has a higher-octane number (106-110) than the latter (91-96). Because of its higher-octane level, ethanol can be burned at a higher compression ratio with a shorter burn time, resulting in less engine knock (Nwufo et al., 2013). Furthermore, ethanol has a higher evaporation enthalpy (1177 kJ/kg at 60° C) than petrol (348 kJ/kg at 60° C) and a faster laminar flame speed (around33 and 39 cm/s at 100kPa and 325K for petrol and ethanol, respectively) (Lynd et al.,1991). Ethanol has a higher volumetric blend than petrol. As a result, heater vaporization ethanol is greater than that of

petrol, increasing power output. Bioethanol is an environmentally friendly oxygenated fuel because it contains 34.7% oxygen, whereas petrol contains no oxygen (Masum et al., 2014). As a result, ethanol has 15% higher combustion efficiency than petrol. In comparison to petrol, ethanol contains a low amount of sulphur, and mixing the two fuels helps to reduce the amount ofsulphur in the fuel as well as the emission of sulphur oxide, which is a carcinogen and can contribute to acid rain (Pranav et al., 2018). Over time ethanol usage in transportation can be noticed prominently (Madhumita et al.2024) in (Fig. 1).

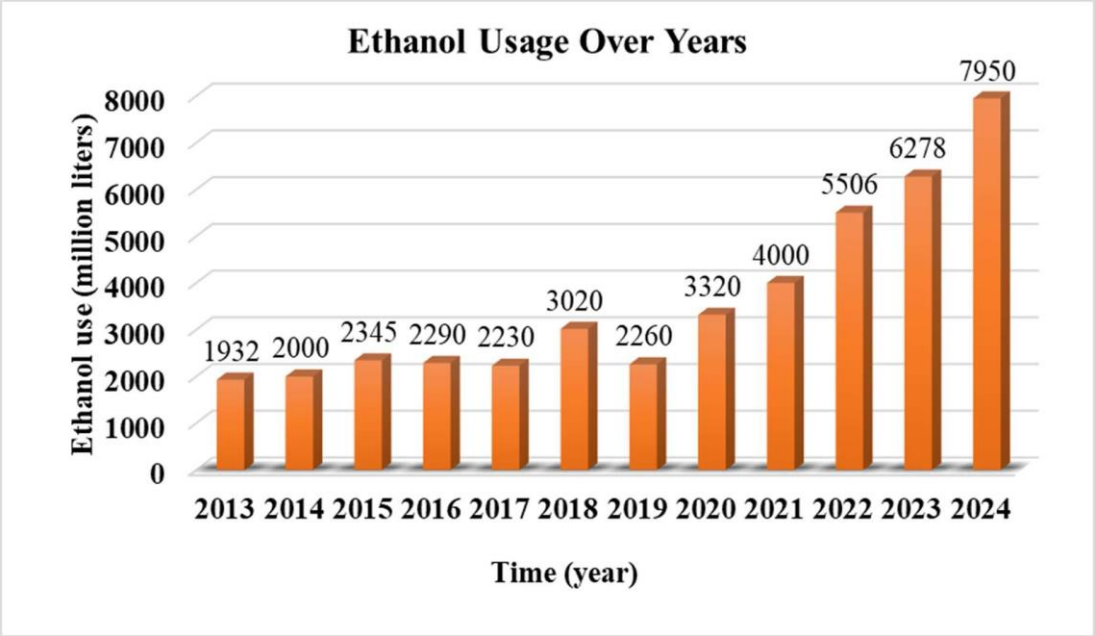


Fig.1 Ethanol demand from 2013-2024

The various raw materials used in the production of bioethanol are classified into four types based on the source of its production (Balat et al.,2011). The first generation of bioethanol is derived from edible crops such as oil seeds, potato, rapeseeds etc (Naik et al.,2010). The second generation is derived from lignocellulosic biomass like sugarcane bagasse, rice straw etc (Sharma et al.,2018). Third generation bioethanol is made from high carbon embedded algal biomasses such as microalgae (Callegari et al.,2020). As the fourth generation biofuel, modified microorganisms such as yeast, microalgae, fungus etc. are used as raw materials to produce sustainable bioethanol (Devi et al., 2023). Due to low yield, high operation cost, unknown factors and health risk third and fourth generations are not favourable for now. Second generation bioethanol production is more preferable due to being non-food grade agricultural waste which is easily available. The production of biofuels often involves crops

or biomass, providing an additional market for agricultural products. This can positively impact rural economies and farmers, offering economic incentives for sustainable farming practices. The development and use of biofuels drive research and technological advancements in areas such as agricultural practices, biotechnology, and renewable energy production (Olaganathan, et al.,2014). This innovation contributes to a more sustainable and efficient energy landscape. Bioethanol can be produced domestically, reducing dependence on imported fossil fuels and enhancing energy security (Ibeto et al.,2011). Local production can also stimulate rural economies by creating jobs in agriculture and biofuel production (Peskett et al.,2007, Horst et al.,2011). Bioethanol usage in India has surged due to government policies like the National Biofuel Policy and the Ethanol Blending Program, aiming to reduce emissions. This involves blending ethanol with petrol, with set targets increasing over time. Ethanol production has risen, utilizing sugarcane, molasses, corn, and alternative feedstocks. Infrastructure expansion, including plant setups and logistics, supports ethanol distribution. Bioethanol offers environmental benefits by curbing emissions and air pollution. Challenges like feedstock availability and infrastructure limitations persist but present innovation opportunities. Over time ethanol usage in transportation can be noticed prominently.

In India, bananas account for more than 20% of all crop land. The banana plant has a shorter life cycle than lignocellulosic biomass derived from wood. The banana plant only produces fruit once during its lifetime, and for every cycle of banana production, four times as much waste as actual fruit is produced (Adsal et al.,2020). Fruit-bunch stems, leaves, pseudostems, and rhizomes are all parts of the abundantly lignocellulosic waste from bananas. Banana pseudostem creates about 73% of the total waste produced after the banana fruit is harvested. Because of its high cellulose (50%), moderate hemicelluloses (30%), low lignin (18%) and pectin (2%) contents (Mohiuddin et al., 2014), banana pseudostem is recognized as an appealing, non-edible cellulosic feed stock suitable for bioethanol production.

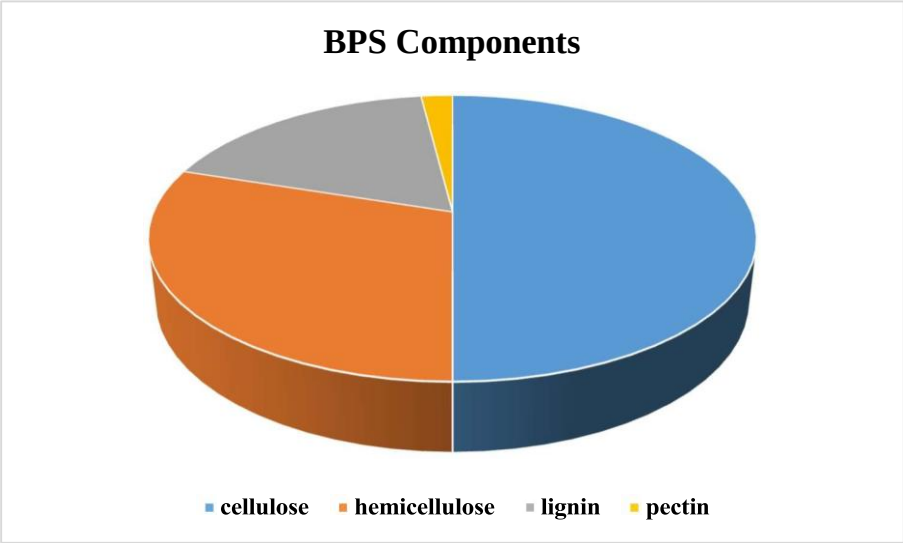


Fig. 2 WBP components

For the past decade banana pseudo- stem has become a prominent feedstock for production of fermentable sugar ultimately leading to biofuel (bioethanol) production. Bioethanol can be processed from banana pseudostem through some steps. First pretreatment, the pretreatment of lignocellulosic biomass is essential for breaking down its complex structure into simpler components. Common pretreatment methods include physical, chemical, biological, combined, and physicochemical approaches (Shirkavand et al.,2016). Physical pretreatment methods like milling and steam explosion increase the surface area of biomass particles, aiding subsequent treatments. Chemical methods such as acid hydrolysis, alkaline hydrolysis, and organic solvent dissolve or break down lignin and hemicellulose, improving cellulose accessibility. Biological pretreatment involves using fungi or enzymes to selectively degrade lignocellulosic components. Combined pretreatment techniques combine different methods to maximize delignification, hemicellulose removal, and cellulose accessibility. Simultaneous saccharification and fermentation (SSF) integrates enzymatic hydrolysis with microbial fermentation for efficient biofuel production. Physicochemical methods like hydrothermal and ionic liquid pretreatment use temperature, pressure, and solvents to break down biomass components.

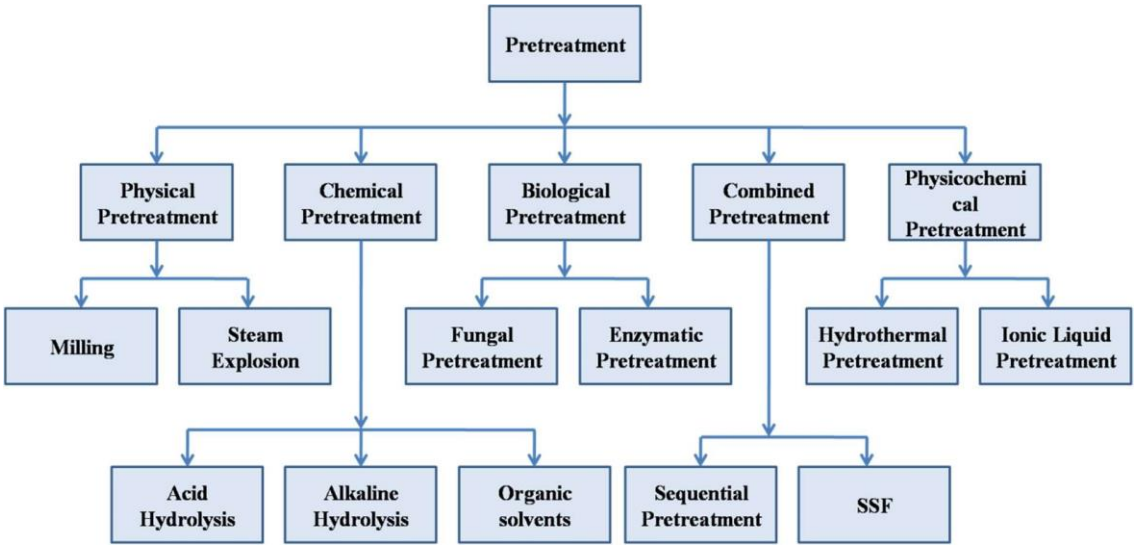


Fig. 3 Flowchart of various pretreatment processes for lignocellulosic biomass

The choice of pretreatment method depends on factors such as biomass type, desired products, economic feasibility, and environmental impact. Various pretreatment methodologies are given in Fig. 3. Evaluation parameters include sugar yield, enzymatic digestibility, and inhibitor formation. Then the holocellulose (cellulose + hemicellulose) part is later converted into fermentable sugar through saccharification or hydrolysis using enzyme or chemical catalyst. Enzymatic hydrolysis of cellulose involves the use of cellulase enzymes, including endoglucanases, exoglucanases, and β-glucosidases, to break down cellulose into glucose and other sugars. Endoglucanases initiate the process by hydrolyzing internal bonds within the cellulose chain, producing shorter polysaccharide fragments. Exoglucanases then further break down these fragments into cellobiose, which is a dimer of glucose. Finally, β-glucosidases convert cellobiose into glucose, which is a fermentable sugar (Van et al.,2007). Catalytic hydrolysis utilizes chemical catalysts to promote the breakdown of cellulose into sugars. Catalysts like mineral acids, solid acid catalysts, and heterogeneous catalysts facilitate hydrolysis by protonating the oxygen atoms in cellulose's glycosidic bonds (Shrotri et al.,2017). This protonation weakens the bonds, making them more susceptible to breakdown and thereby facilitating hydrolysis. This process results in the formation of glucose and other fermentable sugars. Catalytic hydrolysis offers high reaction rates and broader applicability to different biomass but often requires harsh reaction conditions and may lead to the formation of inhibitors.

Ezymatic Hydrolysis Vs Catalytic Hydrolysis

Catalysts are materials that enhance reaction rates without undergoing consumption. They play a crucial role in chemical processes. Positive catalysis speeds up reactions by reducing activation energy, while negative catalysis is vital for regulating chain reactions. Background knowledge is a determining factor in choosing between bio- and chemical catalysts. Chemical catalysts typically consist of metals, as many metals possess numerous electrons that exhibit a degree of flexibility regarding their proximity to the central atom. This flexibility enables metals to utilize these electrons to facilitate reactions, reclaiming them once the reaction concludes. For instance, iron-based catalysts are utilized in the production of ammonia (the Haber-Bosch process), while nickel catalysts are employed in the synthesis of saturated fats.

Biological catalysts operate on a distinct principle from chemical catalysts. Instead of being metallic with electrons that behave flexibly, biological catalysts are intricate large molecules known as enzymes. Enzymes feature specific pockets where reactants can fit snugly. Once trapped inside, the enzyme facilitates the reaction either by establishing temporary bonds with the reactants to facilitate their assembly or by merely holding them in close proximity for them to react and produce the desired product.

The majority of enzymes are located within living organisms, enabling them to function effectively without requiring high temperatures. Conversely, metal catalysts often necessitate an initial energy input to initiate the reaction. Enzymes have specific temperature thresholds for optimal functionality, with most denaturing if heated significantly beyond their ideal temperature (typically around 40 degrees Celsius, although certain bacterial enzymes can operate at temperatures as high as 100 degrees Celsius) (Pinney et al.,2021). This characteristic presents significant advantages in scenarios like biological washing powders, where lower temperatures suffice for reactions, conserving energy and allowing for washing at cooler temperatures. However, in some industrial processes, elevated temperatures are essential to enhance reaction rates, rendering cooling everything down to 40 degrees impractical.

- Choice of solvent

Another factor influencing the choice of catalyst is the necessity to achieve acceptable yield and purity in product isolation. Despite advancements in using enzymes with organic solvents and poorly soluble substrates in aqueous media, challenges persist. Conversely, if the product has high water solubility, isolating the desired material can be notably challenging. Chemical

reactions typically benefit from a variety of solvent systems available for the transformation and subsequent isolation.

Enzymes are highly specific compared to chemical catalysts. Due to the precise fitting of reactants into enzyme pockets, each enzyme can only catalyze specific molecules. Designing enzymes to accommodate desired reactants is complex due to their large and intricate nature. While this specificity is advantageous for applications like biological washing powders, where enzymes evolved to tackle various stains, it poses challenges in chemical processes. Few organisms have evolved to address tasks such as removing toxic gases from petrol or synthesizing sulfur dioxide (Ager, D., 2012).

- Scale up

Scaling up chemical catalytic reactions typically follows standard process chemistry procedures. Synthesizing ligands and transition metal catalysts usually poses few challenges, as the quantities involved are much smaller compared to the reaction itself. However, enhancing specificity and efficiency often necessitates the preparation and testing of new catalysts, which can be a time-intensive process.

In contrast, biocatalytic approaches offer the flexibility to modify original enzymes through genetic alterations and rapid screening, addressing selectivity, stability, and other concerns. Nevertheless, these studies can also be time-consuming and may demand more resources compared to simply creating a new ligand (Ager, D., 2012).

- Cost and Speed

The criteria of cost and speed also play significant roles in selecting a catalyst system. In the initial stages of drug candidate development, speed is crucial, while cost remains an important consideration. Precedence and catalyst availability are key factors influencing the choice.

As projects progress to larger scales, the preference may shift from chemical methods to biocatalytic ones. Biological routes often prove cost-effective for commercial production. However, it's essential to note that the catalytic step typically forms part of a synthetic sequence. Preparation of the substrate for the catalytic step and conversion of the product to the final target molecule are necessary steps (Ager, D., 2012).

- An Exclusive Approach

Biocatalysts can alter lignin by reducing its hydrophobicity, thereby improving saccharification by reducing non-productive cellulase binding. The high selectivity of biocatalysts, along with reduced generation of toxic by-products, high product yields, decreased chemical requirements, lower energy consumption, and mild environmental conditions, make them appealing and sustainable options. However, their high cost, slower reaction rates, lower product yields, reduced recovery rates, and challenges in scalability limit their utilization (Sun SL et al., 2019, Sabiha-Hanim et al., 2018).

Chemical catalysts are appealing due to their easy product separation, moderate recyclability, high availability, and favorable physicochemical properties like bronsted acidity and hydrothermal stability. However, they pose sustainability challenges due to significant catalyst requirements, difficulties in product separation, poor resistance to mass transfer, instrument corrosion, waste effluent treatment issues, and catalyst separation challenges. Additionally, the need for elevated temperatures (150-190ºC) and long reaction times (10-24 hours) raises energy consumption and costs. Huang et al. (2013) noted that liquid HCl has low recyclability in large-scale processes.

Sulphonated activated carbon, as mentioned by Wang et al. (2014), can achieve a 41% glucose yield but suffers from thermodynamic instability during reactions. Luo et al. experimented with carbonaceous solid acid catalysts for higher biofuel yields in 2017, highlighting the need for smaller substrate sizes for effective action, which in turn increases production costs.

While photocatalysts like TiO2 enhance hydrolysis by absorbing light and accelerating catalyst activity, they are not sustainable due to slow oxidation rates for many pollutants, agglomeration, difficult separation processes, and low recycling rates. Additionally, the reformation of biomass with photocatalysts at ambient temperature and in highly basic media increases biofuel production costs.

Washing and detoxification is crucial for removing some toxic or inhibitory component from the fermentable sugar. Later the fermentable sugar is converted into bioethanol through microbial fermentation and the pure ethanol is collected through distillation process.

Due to possible reusability of enzymes and increase in solidity, pH maintenance, stringency, sustainability in higher temperature and anti-microbial properties immobilization is getting popular in resent studies. Immobilization is a technique where enzymes or cells or amino acids are being trapped or attached to a solid insoluble material. By changing the structure of support bio catalytic efficiency can be improved. There are numerous ways to immobilize enzymes with particles, including physical adsorption, entrapment, and covalent binding (Chen et al., 2015). Even though enzyme loading per unit mass of support is often minimal, nonporous materials with enzyme attached are subject to minimum diffusion limitations. However, porous materials allow for increased enzyme loading at the expense of a much higher substrate diffusional constraint. The efficiency of immobilized enzymes is often improved by the reduction in the size of the enzyme-carrier materials. Additionally, smaller particles can offer more surface area for the attachment of enzymes in the case of surface attachment, resulting in a higher enzyme loading per unit mass of particles. However, issues with recovery, such as centrifugation or filtration, could limit the use of immobilized enzyme on particles in industrial biotechnology. Magnetic particles (MNPs) are easily recovered for reuse and have the potential to be useful supports for bioactive substances like peptides, enzymes, antibodies, and nucleic acids. They generally have low toxicity, but their key benefit is that they can be easily separated from reaction mixtures with the help of magnets (Khoshnevisan et al., 2011). However, no scientific report has been published on the development and application of magnetic particles with photo catalytic properties in immobilization of cellulose enzyme.

Radiation plays significant role in pretreatment process. Study by Roy Choudhury et al.,2021 shows that using electromagnetic radiation the delignification can be more effective than the conventional thermal reactor. Near-infrared (NIR) radiation has emerged as a valuable tool in the delignification process of lignocellulosic biomass, offering several advantages over traditional methods. Delignification, the removal of lignin from biomass, is a critical step in the production of various bio-based products, including biofuels, biochemicals, and biomaterials. Near-infrared (NIR) radiation occupies a fascinating niche within the electromagnetic spectrum, lying just beyond the visible light spectrum and before the realm of microwaves. Its wavelengths range from approximately 700 meters to 1 millimeter, nestled between the visible light spectrum and the longer wavelengths of infrared radiation. Near-infrared (NIR) radiation enables selective heating of lignin-rich regions, preserving cellulose and hemicellulose integrity, enhancing targeted delignification while minimizing energy

consumption. Its controlled process parameters allow fine-tuning for optimal outcomes, ensuring efficient lignin removal (Barman et al.,2019). Environmentally friendly, NIR delignification reduces chemical usage and waste generation, offering a clean and sustainable solution. Versatile across various biomass types, from agricultural to municipal waste, NIR expands biomass application possibilities. Integration with other technologies, like enzymatic hydrolysis or chemical conversion, enhances overall efficiency and valorization of biomass resources.

Bioethanol fermentation transforms biomass sugars into ethanol via microbial action, mainly by yeast or bacteria. Key factors affecting yield include feedstock composition, microbial strain, fermentation conditions (temperature, pH), nutrient availability, inhibitors, and enzymatic hydrolysis for lignocellulosic materials, process optimization, and management of co-products / by-products (Tse et al.,2021). Feedstock diversity influences sugar content and thus ethanol yield. Microbial strains like Saccharomyces cerevisiae are pivotal, with ongoing research for enhanced traits. Optimal fermentation conditions and nutrient levels are critical for microbial growth and ethanol output. Various fermentation parameters including temperature, pH, agitation, and oxygenation influence microbial growth and ethanol production. Optimal fermentation conditions vary depending on the microbial strain and feedstock used. For example, yeast fermentation typically occurs at temperatures ranging from 25°C to 35°C and pH levels of 4.0 to 5.0 (Abeln et al.,2020). Inhibitors from biomass or processing can impede fermentation, demanding detoxification strategies. Enzymatic hydrolysis of lignocellulosic feedstocks precedes fermentation, requiring careful management. Process optimization, including fermentation time and vessel design, enhances efficiency. Co-products or by-products management is vital to prevent resource competition and maximize ethanol output. Through meticulous attention to these factors, bioethanol producers can optimize fermentation processes, contributing to sustainable fuel and chemical production. Ongoing research seeks to refine techniques and address challenges, further elevating bioethanol production efficiency.

Life Cycle Assessment (LCA) is a technique to assess the environmental aspects and potential impacts associated with a product, process, or service throughout its entire life cycle. This includes extraction and processing of raw materials, manufacturing, distribution, use, repair and maintenance, and disposal or recycling. LCA is crucial for green technologies as it offers a holistic view of their environmental impact from inception to disposal. It identifies key

stages where environmental effects are most pronounced, aiding engineers to focus on optimizing these critical areas. LCA facilitates comparative analysis, aiding decision-makers in selecting the most eco-friendly option among alternatives. By shedding light on the environmental consequences of design choices, LCA informs the development of greener technologies. Its results also support policy-making by providing evidence-based assessments for governments and regulatory bodies. Moreover, LCA findings can be effectively utilized for communication and marketing purposes, highlighting the environmental benefits to stakeholders. Importantly, LCA is an iterative process, enabling continuous improvement by monitoring environmental performance and identifying areas for optimization over time (Barman et al.,2024).

In this study, waste banana pseudostem (WBP) was effectively delignified using peracetic acid under visible range irradiations from a carbon filament. Cellulase immobilized magnetic photo-active iron (CIMPI) was synthesized using the glutaraldehyde activation covalent bonding method. Characterization studies of CIMPI were conducted confirming its photoactive nature. CIMPI was then utilized for sustainable photoactive chemo-bio-saccharification of pretreated WBP (PWBP) in a carbon infrared irradiated vibrating batch reactor (CIIVBR) (100 W, 750–1400 nm). This process was optimized using an L9 Taguchi experimental design (L9TED), achieving a maximum fermentable sugar yield of 73.40 wt. % under mild reaction conditions, thereby highlighting the superiority of the CIIVBR which could save 80% energy compared to the conventional batch reactor (CBR) at the optimal condition. This work also presents subsequent fermentation of the resulting FS using dry yeast viz. Saccharomyces cerevisiae to substantial bio-ethanol yield (maximum of 24.2g/l) giving an efficiency of 79.08 %. The overall technology also focussed on the sustainability, and minimal environmental impact by Life cycle assessment (LCA) study. Similar chemo-biocatalyst cellulase immobilised photoactive tin (CIPSn) was synthesized using tin oxide by calcination of tin chloride. Xrd, TGA and FTIR were done for CIPSn catalyst analysis. After pretreatment of pineapple leaves CIPSn was used for saccharification and the process was optimized using L9TED. Maximum 56.7% FS yield can be obtained.

CHAPTER 3

LITERATURE REVIEW

Chemo-enzymatic conversion of lignocellulosic biomass (Banana pseudostem) to bio-ethanol

Immobilization of cellulase enzyme on iron oxide particles

- Khoshnevisanet et al.,2017: This study shows that, enzyme immobilization on solid supports is the most effective method for achieving high catalysis and reusability. The use of particles as inert supports for the immobilization of enzymes is among these. Given how costly it is to separate sized solid supports from reaction medium and recycle them, MNPs may be the perfect particles for immobilizing enzymes because they are readily retrieved through the application of an external magnetic field. Up till now, varieties of MNPs—such as polymer brushes, enzymogels, magnetic chitosan particles, silica-coated MNPs, amine and aldehyde functionalized MNPs, etc.—have been altered to be employed as cellulase carriers.
- Zang et al.,2014: In this study, chitosan was coated onto the surface of Fe3O4 particles to create magnetic chitosan supports. Cellulase was then effectively immobilized on Fe3O4-chitosan particles by gluteraldehyde activation method. It is simple to separate the immobilized cellulase from the reaction mixture due to its high magnetic sensitivity (46.6 emu/g). For immobilized cellulase, the ideal pH was 5, and the ideal temperature was 50°C. On Fe3O4-chitosan particles, cellulase was discovered to be present in as much as 112.3 mg/g, with an activity of 5.23 IU/mg. Compared to free cellulase, the immobilized form of the enzyme had better temperature stability. After ten rounds, 50% of the immobilized cellulase's original activity was still present. Meanwhile, after ten cycles, the glucose productivity during the course of a day continued to be more than 80% of the initial value. This finding indicated that the Fe3O4-chitosan support was appropriate for covalently immobilizing cellulase and large-scale glucose production could benefit from the use of the resulting immobilized enzyme.
- Khoshnevisan et al.,2011: In this study through physical adsorption, the cellulase enzyme was bound (ionic bound). The successful binding of cellulase (endoglucanase) onto the particle was verified by FTIR spectroscopy, and binding efficiency was calculated using the Bradford method at 95%.The size and structure of cellulase on commercial superparamagnetic particles were studied using TEM and DLS techniques. Using CMC as the substrate, the highest enzyme activity was measured and found to be 0.1 unit (μmol/min ml). Cellulase was able to bind to particles at a rate of 31 mg/g. When compared to the free enzyme, the immobilized enzyme's stability increased. Overall, our study demonstrated that

physical adsorption to the magnetic particles increased the stability and activity of the cellulase enzyme. This indicated that mounted enzyme on magnetic beads would have a wide range of applications. It would enable long-term preservation across a wider pH and temperature range and allow for the enzyme's magnetic recovery for further use or product purification.

- Lima et al.,2017: This study investigated cellulase immobilization on magnetic particles within polymeric spheres. The support, characterized for morphology and magnetic behavior, demonstrated superparamagnetic properties with an average diameter of around 150 nm. Immobilized cellulase displayed increased temperature stability and remarkable reusability, maintaining 69% of its initial activity after eight cycles. The magnetic support exhibited promise for efficient cellulase immobilization, enabling convenient biocatalyst recovery using a single magnet.
- Ladole et al.,2017: This study successfully investigated the impact of ultrasound in a temperature-controlled ultrasonic bath on enzyme@MNPs activity. Cellulase@MNPs exhibited a maximum activity recovery of 80%, and when subjected to optimized ultrasound conditions, it demonstrated a 3.6-fold increase in activity compared to non-irradiated immobilized cellulase. Notably, the catalytic efficiency of cellulase@MNPs improved with increased V_{max} and decreased K_m during sonication, indicating enhanced substrate affinity. Changes in the secondary structure of both free and immobilized cellulase were observed pre and post-sonication. The hydrolytic efficiency of immobilized cellulase with sonication surpassed that without, showcasing its increased effectiveness in biomass conversion.
- Selvam et al.,2016: Fe3O4 magnetic particles were synthesized through co-precipitation of Fe2+ and Fe3+ ions in an ammonia solution, followed by hydrothermal treatment. Cellulase was immobilized onto these magnetic particles using glutaraldehyde activation. Optimization of key variables, such as magnetic particle concentration, glutaraldehyde concentration, enzyme concentration, and cross-linking time, was achieved through response surface methodology and Box-Behnken design. Statistical contour plots were generated to understand the relationship between particles and enzyme activity. Characterization using scanning electron microscopy, X-ray diffraction, and Fourier-transform infrared spectroscopy revealed size, structure, morphology, and enzyme binding onto the particles. The stability and activity of the immobilized cellulase were evaluated under various conditions, including pH, temperature, reusability, and storage stability.

Comparative analysis with free cellulase demonstrated enhanced stability and activity in the immobilized cellulase.

- Mubarak et al.,2014: In this study, cellulase enzyme immobilization onto multi-walled carbon tubes (MWCNTs) was accomplished through physical absorption. A 2 mg/mL solution of functionalized MWCNTs was prepared by dispersing 4 mg of MWCNTs into 2 mL of 0.05 M phosphate buffer (pH = 7.0). The solution was mixed and incubated in an incubator shaker at 30°C and 200 rpm for 2.5 hours. After incubation, the MWCNT–cellulose composite was separated by centrifugation and washed multiple times with fresh phosphate buffer to remove unbound protein. The washed composite was air dried for 24 hours to yield the immobilized MWCNT–cellulase conjugate. FTIR spectroscopy and FESEM confirm the successful immobilization of cellulase enzyme. The optimal enzyme concentration of 4 mg/mL achieves approximately 97% enzyme loading. UV–visible spectroscopy identifies pH 5 and 50°C as the optimal reaction conditions for immobilized cellulase. The MWCNT–cellulase composite retains 52% of its cellulase activity after six cycles of the CMC analysis.
- Han et al.,2018: In this research, graphene oxide (GO) decorated with 4-arm PEG NH2 on magnetic Fe3O4, termed GO@Fe3O4@4arm PEG NH2, was synthesized and extensively characterized using various techniques. The saturation loading capacity of GO@Fe3O4@4arm PEG NH2 (with MW 5K and 10K) towards cellulase was determined to be 429 mg/g and 575 mg/g, respectively. The immobilized cellulase exhibited improved thermostability, storage stability, and reusability compared to the free enzyme. Both forms of immobilized cellulose (MW 5K and 10K) retained approximately 57% and 60% of their initial activity after 3 hours at 70°C and 47% and 50% after 30 days of storage at room temperature. After eight cycles of reuse, they retained 40% and 45% of their initial activity, respectively. In practical applications, the immobilized cellulase significantly outperformed the free enzyme, with glucose production reaching 2.04–2.83 times higher levels when the enzyme loading ranged from 2–8 mg, showcasing the potential of this biocatalyst.

Banana pseudostem conversion towards total fermentable sugar leading to bioethanol

- Gatdula et al.,2021: This research was conducted SSF using rice straw and banana pseudostem, employing Kluyveromycesmarxianus and commercial enzymes after chemical treatment. A consistent 10% vv -1 inoculum loading was maintained with a nutrient-enriched solution. Only reaction time significantly affected ethanol concentration. Pre-treated rice

straw achieved 6.30+0.44 gL -1 ethanol at 45°C, 48-hour reaction time, and enzyme loading of 30 FPUg -1. Banana pseudostem yielded 5.35+0.29 gL -1 ethanol at 35°C, with a 24-hour reaction time and the same enzyme loading. This study highlights K. marxianus' potential for bioethanol production from lignocellulosic materials via SSF, suggesting it as a Saccharomyces cerevisiae alternative.

- Sukmaningtyas,2018: In this study different pretreatment methods, including autoclaving of banana pseudostem in steam and NaOH solutions of varying concentrations (0.5N, 1N, 1.5N, 2N) for 90 minutes, were utilized. Subsequently, enzymatic hydrolysis was conducted for 24, 48, and 72 hours. Simultaneous saccharification and fermentation (SSF) employing cellulase enzyme and Saccharomyces cerevisiae yeast lasted 120 hours. Increasing NaOH concentration during pretreatment decreased lignin content while increasing cellulose content. The lowest lignin content recorded was 11.44%, with the highest cellulose content reaching 51.66%. The highest sugar content obtained was 29.8 g/L (with pretreatment using 2N NaOH solution, followed by 72 hours of hydrolysis). The maximum bioethanol yield of 4.32 g/L was achieved from pretreated banana pseudostem using 2N NaOH solution.
- Souza et al.,2014: This study explored bioethanol production by Saccharomyces cerevisiae using banana pseudostem residue as a fermentation substrate. Two pre-treatment methods were assessed: (a) fresh biomass cut into 1 mm pieces and (b) dry and milled biomass. Pre-treatments involved H2SO4 (2% m/m) and NaOH (3% m/m) at 120 ºC for 15 minutes. Enzymatic hydrolysis using Novozymes® complex (cellulase, beta-glucosidase, xylanase) followed (24 h, pH 5.5, 45 °C). The highest glucose yield (79.5±4.4%) was achieved with NaOH-treated fresh biomass. Fermentation of hydrolyzed liquor from dry biomass with H2SO4 (RS ≤ 62.1 g/L) resulted in ethanol production (22.1±0.8 g/L), with YP/RS = 0.47±0.03 g/g, QP = 1.83±0.12 g/L.h, and EP = 80.4±0.12%.
- Ingale et al.,2014: This study employed Aspergillus ellipticus and Aspergillus fumigatus strains to produce cellulolytic enzymes on sugarcane bagasse and co-cultured them for fermentation on banana pseudostem to degrade holocellulose. The resulting hydrolysate, after alkali and microbial treatments, was fermented by Saccharomyces cerevisiae NCIM 3570 to yield ethanol. Fermentation of the cellulosic hydrolysate (4.1 g%) yielded maximum ethanol (17.1 g/L) with an 84% yield and productivity of 0.024 g%/h after 72 hours. The study explores critical aspects of fungal pretreatment for saccharification of cellulosic substrates, highlighting the potential of A. ellipticus and A. fumigatus for ethanol production by S. cerevisiae NCIM 3570.

- Silva et al.,2014: This research aimed to enhance pre-treatment methods for converting banana pseudostem into bioethanol. Microwave-assisted liquid hot water and alkaline (sodium hydroxide) pre-treatments were conducted, varying severity factors and NaOH loading. Optimal conditions from both methods were chosen based on enzymatic hydrolysis yields for subsequent fermentation via simultaneous saccharification and fermentation (SSF) at 25℃ for 120 hours. The liquid hot water pre-treatment achieved a higher ethanol yield (95% of theoretical yield) compared to the alkaline pre-treatment (92%). Liquid hot water is favored for its economic and environmentally friendly nature, while the alkaline method poses challenges due to potential pollution from sodium discharge.
- P et al.,2018: The project aims to produce bioethanol from banana waste using Saccharomyces cerevisiae. Pseudostem, rachis, and banana peels were utilized for saccharification and fermentation. Two methods were employed for bioethanol production to optimize industrial transferability. Initial HCl pretreatment broke down lignin content, followed by hydrolysis using thermamyl and amyloglucosidase enzymes. Operating conditions for α-amylase included 90-100°C temperature, pH 4.5, and 0.1% enzyme concentration, while amyloglucosidase operated at 50-60°C and pH 4.5. After saccharification, fermentable sugar concentration was adjusted to 11% for yeast fermentation. Distillation of fermented solution yielded 87ml distillate containing 56% ethanol based on specific gravity.
- Araguirang et al.,2020: The study explored the potential of M. acuminata x balbisiana pseudostem for second-generation ethanol production. Optimization of solid loading, incubation time, and enzyme amount revealed that incubation for 20 hours with 15 g solid loading and 0.55% enzyme concentration yielded the highest fermentable sugar. Scaling up saccharification increased sugar concentration in the hydrolysate. Activated carbon detoxification enhanced fermentation performance, indicating a promising pathway for ethanol production.
- Legodi et al.,2021: The study investigated various pretreatment methods (NaOH, H2SO4, liquid hot water) on banana pseudostem (BPS), resulting in cellulose availability of 52%, 48%, and 25% respectively. Saccharification of pretreated BPS with crude enzymes from Trichodermaharzianum and T. longibrachiatum released 3.8 to 21.8 g/L and 5.4 to 43.5 g/L glucose, respectively. Ethanol production via separate hydrolysis and fermentation (SHF) of alkaline pretreated BPS hydrolysate using Saccharomyces cerevisiae yielded

17.6 g/L ethanol. The study demonstrates BPS as a cost-effective substrate for bioethanol production.

- Dilkushi et al.,2024: The study explored cellulase production using Trichoderma and Aspergillus species via solid-state fermentation with banana pseudostem (BPS) as a carbon source. Optimal conditions included 75% moisture content of untreated BPS, at 30°C, with Trichoderma longibrachiatum LMLSAUL 14-1 exhibiting maximum cellulase activity. Pre-treatment of BPS, particularly with NaOH or H2SO4, enhanced enzyme production, with Aspergillus fumigatus LMLPS 13-4 and T. harzianum LMLBP07 13-5 showing notable β-glucosidase activity on acid and alkali-treated BPS, respectively. Co-culturing T. harzianum LMLBP07 13-5 and A. fumigatus LMLPS 13-4 improved endoglucanase production. These findings highlight BPS as a promising, cost-effective substrate for cellulase production, leveraging waste from the banana industry.
- Laltha et al.2024: The study investigated novel pretreatment methods, M-ITS and M-PWW, utilizing iodized table salt and Kraft paper wastewater for enhancing sugar recovery from banana pseudostem. Optimization showed slightly higher fermentable sugar and glucose yields with M-ITS (0.515 g/g and 0.433 g/g) compared to M-PWW (0.498 g/g and 0.413 g/g). Despite comparable yields to chemical-based methods, M-PWW demonstrated higher efficiency as a waste-based approach, requiring fewer pretreatment cycles. These findings offer a promising avenue for lignocellulosic pretreatment, potentially reducing reliance on costly chemicals and fresh water, promoting a waste treating waste approach.
- Samara et al.,2024: This study investigates enzymatic hydrolysis of alkaline microwave-assisted pre-treated banana stem cellulose, varying hydrolysis times (5-45 h) and enzyme-to-substrate ratios (1:1 to 1:10). Pre-treatment enhances cellulose accessibility by subjecting biomass to 5% KOH for 30 min followed by microwave exposure at 300 W for 5 min. Results show significantly improved hydrolysis efficiency, with highest fermentable sugar concentration (1.3 mg mL−1) achieved at 1:1 substrate-to-enzyme ratio and 45 h hydrolysis duration. These findings highlight the potential of integrated pre-treatment strategies for sustainable biorefinery applications, advancing lignocellulosic biomass utilization for biofuel and biochemical production from banana stem waste.
- Shaj et al.2024: Bioethanol production from banana lignocellulosic biomass (raw peel, ripe peel, pseudostem) was explored, with ripe peel showing the highest total fermentable sugar content (21.98%). Acid pretreatment yielded higher lignin removal and increased sugar content compared to alkali treatment. Fermentation processes (SHF, SSF,

SBB) using Saccharomyces cerevisiae resulted in 6.63% ethanol from untreated banana raw peel. Introduction of a native cellulolytic microorganism alongside Saccharomyces cerevisiae in SBB enhanced bioethanol production to 6.88%. This study marks the first use of a native microorganism for improved cellulose degradation in banana biomass, promising higher bioethanol yields.

CHAPTER 4

RESEARCH GAPS

4. Research gap

Based on the literature review some adversities have been noted:

1) Effective lignin separation not been reported.

2) Fermentable sugar yield from pretreated BPS is relatively low.

3) Using acidic pretreatment causes severe loss of fermentable sugar and is also detrimental for the biomass yield.

4) Effect of enzyme dosage harnesses the bioethanol yield.

5) The temperature and energy requirement is reported high making it energy intensive technologies.

6) The saccarification and fermentation time required was more, which is not beneficial for the mass production.

7) Fe_3O_4 is regarded as a prominent magnetic particle exhibiting photo catalytic property, the synergistic activity with immobilized cellulase has not been reported yet.

8) It has been seen that strong acid pretreatment, long time durations, high reaction conditions can cause harm to the product in the form of inhibitors thereby reducing the yield.

9) The chemically pretreated drained water in turn affects the eco-system making it hazardous for the environment.

10) Though high enzyme loading results in comparatively higher yield, still it is not a desirable step due to the higher economic value of the enzyme making the whole procedure a costly process.

Hence the expected outcome of this project will be to develop a hybridized enzymatic-chemo-catalytic conversion of cellulosic biomass (banana pseudo-stem) towards bioenergy (bioethanol) and another cellulosic biomass (pineapple leaves) towards FS through cost-effective, energy-efficient and eco-friendly pathway.

CHAPTER 5

AIMS & OBJECTIVES

5.1 Aims & Objectives for WBP conversion to Bio-ethanol

- Collecting banana pseudostem waste from the local market
- Synthesis of magnetic photo active chemo-bio catalyst (CIMPI)
- Pre-treatment of waste banana pseudostem to remove lignin and collecting holocellulose
- Production of fermentable sugar from pretreated banana pseudostem using CIMPI
- Fermentable sugar yield optimization using taguchi orthogonal L9 design array
- Production of bio ethanol under anaerobic condition using dry yeast
- Less expensive production process
- Less energy intensive process
- Process intensification by near infrared radiation
- Efficiency of carbon infrared irradiated vibrating batch reactor (CIIVBR) over conventionally heated batch reactor (CBR)
- Less harmful environmental impact
- Reusability analysis of chemo-bio catalyst

5.2 Aims & Objectives for PL conversion to FS

- Collecting pineapple leaves from the farm house
- Synthesis of magnetic photo active chemo-bio catalyst (CIPSn)
- Pre-treatment of pineapple laves to remove lignin and collecting holocellulose
- Production of fermentable sugar from pretreated pineapple leaves using CIPSn
- Fermentable sugar yield optimization using taguchi orthogonal L9 design array

CHAPTER 6

MATERIALS & METHODS

6. Materials and methods

6.1 Materials for production of Bio-ethanol from WBP

- Banana pseudo-stem waste (WBP) was collected from local market of Jadavpur, Kolkata, West Bengal, India.
- Deionized water from Abhishek Chemicals Ltd.
- D (+) – Glucose from Himedia Laboratories Pvt. Ltd.
- Ethanol from Tedia High Purity Solvents.
- Ammonia solution (99%),
- Glacial acetic acid (99-100%),
- Hydrogen peroxide (30%),
- DNS,
- Iron oxide (II, III) particles,
- Cellulase enzyme,
- Gluteraldehyde,
- APTES,
- Acetonitrile etc. were obtained from Merck (India).

6.2 Materials for production of FS from PL

- Pineapple leaves (PL) was collected from farm house near Kolkata, West Bengal, India.
- Deionized water from Abhishek Chemicals Ltd.
- D (+) – Glucose from Himedia Laboratories Pvt. Ltd.
- Glacial acetic acid (99-100%),
- Hydrogen peroxide (30%),
- DNS,
- Cellulase enzyme,
- Gluteraldehyde,
- APTES,
- $SnCl_2$ etc. were obtained from Merck (India).

6.3 Methods for production of Bio-ethanol from WBP

6.3.1 Physical pretreatment of waste banana pseudo-stem

Waste banana pseudostem (WBP) was collected and washed with deionised water thoroughly. It was cut evenly and then air dried in a hot air oven at 90° C for 4h. The dried biomass was then ground in a grinder and mechanical sieving was done to obtain biomass in a particle range of around 300 mesh size. For an effective delignification process modified infrared irradiated peracetic acid treatment was done. (Roy Choudhuryet al. 2021) and AFEX treatment was done.



Fig.4 Hot air oven

6.3.2 AFEX Pre-treatment

At first 10g of sieved banana pseudo stem was weighted and 100ml deionised water was measured and mixed in a two neck round bottle flux. Then 10ml of NH_4OH was transferred into the mixture. A condenser was fitted in one neck of that two neck flux and stirred in a bioreactor integrated with near infrared radiation (IRSBB) (100 W, 750–1400 nm) at 70^0C for 30 min maintaining a speed of 500-400 rpm. The obtained biomass was then filtered and hot water washed to remove the excess ammonia after which it was oven dried at 80^0C to get the biomass mix with holocellulose content.

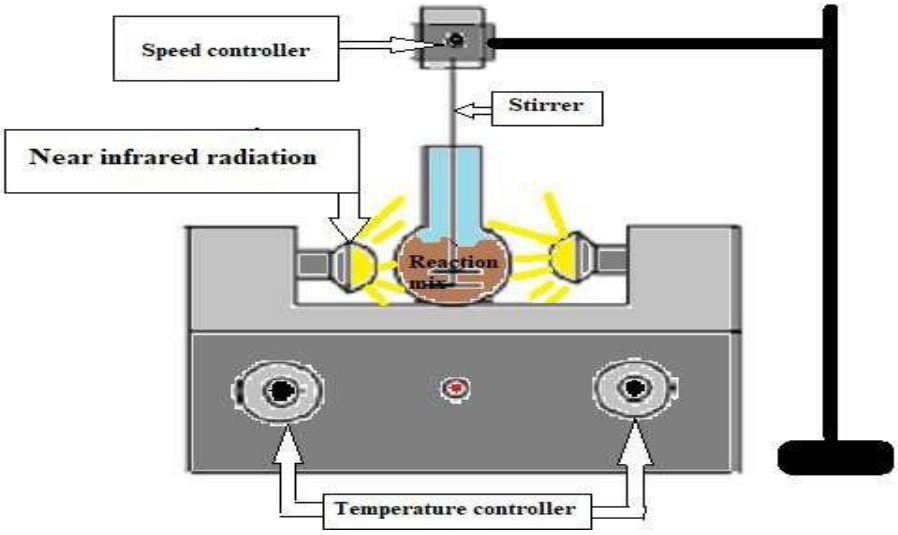


Fig.5 Image of IRSBB

6.3.3 Chemical pretreatment of waste banana pseudo-stem

At first 10 g of sieved WBP was weighed and 10 ml of peracetic acid was mixed in a one-neck round bottle flux. 60 ml of glacial acetic acid was then transferred into the mixture. The mixture was then reacted in CIIVBR (100 W, 750–1400 nm) at 90˚ C for 150 min maintaining a speed of 800-900 rpm. Vacuum filtration was conducted to separate the biomass and a hot water wash was done to remove peracetic acid. The separated lignin was collected for further quantification. The filtrate was oven-dried at 80 ˚C to get the dried biomass. The anthrone approach (Table.1) was utilised to conduct a compositional analysis of the WBP and PWBP.

Table.1 Compositional analysis of WBP and PWBP

Compositional analysis*	WBP (wt. %)	PWBP (wt. %)
Cellulose	50.43	49.3
Hemicellulose	29.28	15.1
Lignin	17.86	1.76

Others	2.43	0.02

* Compositional analysis was done based on Anthrone method [Ludwig et al. 1956]

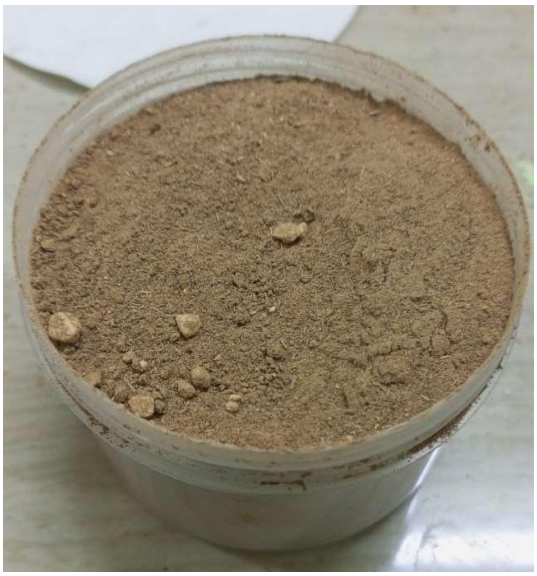


Fig.6 WBP before pretreatment



Fig.7 Pretreated WBP



Fig.8 Hot water washing of PWBP

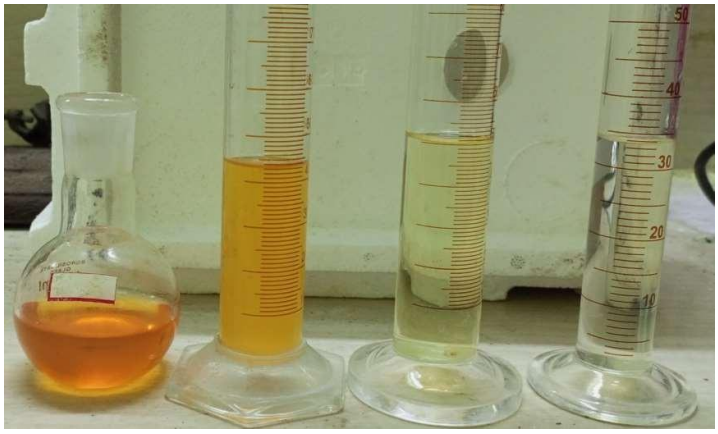


Fig.9 Isolation of lignin

6.3.4 Cellulase immobilization on magnetic photo-active iron particles

At first iron oxide (II, III) particles were washed with 0.1M citrate buffer solution and sonicated in an ultrasonic homogenizer (TAKASHI- U250) for 10 minutes to disperse particles homogeneously. Then the iron oxide particles were collected using a magnet. 7 ml of 1M glutaraldehyde solution was added and incubated in a carbon infrared irradiated vibrating batch reactor (CIIVBR) (100 W, 750–1400 nm) at 37° C for 1h at 120 rpm for activation of iron oxide particles. The activated particles were collected with a magnet and washed with 0.1M carbon infrared irradiated vibrating batch reactor citric acid buffer solution to remove excess glutaraldehyde from the mixture. Then the cellulase enzyme suspended in 0.1M citrate buffer was mixed with 3-APTES and incubated with activated magnetic particles at 37° C for 20h. The cellulase immobilized magnetic-photoactive iron (CIMPI) was collected with a magnet and washed with buffer solution which was then centrifuged at 4°Cfor 15mins at 4000rpm.The unbound enzyme was separated and the immobilized enzymatic-chemo catalyst was further vacuum dried for complete drying of the sample. The CIMPI was stored under refrigerated conditions for further application and characterization.

The binding efficiency of cellulase was determined using the following formula (Abraham et al., 2014).

$$\text{Binding efficiency (\%)} = \frac{\text{Total amount of protein bound}}{\text{Total amount of protein added}} \times 100 \ldots\ldots (1)$$

6.3.5 Saccharification of pretreated waste banana pseudostem (PWBP) with free cellulase enzyme

1g of peracetic acid treated PWBP were taken in a round bottle one neck flask and 30ml deionised water was then transferred in the flask. 5ml of acetate buffer was added after which 1ml of cellulose enzyme was given in the mixture with a micropipette. The mixtures were then put into a carbon infrared irradiated vibrating batch reactor (CIIVBR) (100 W, 750–1400 nm) at 40^0 C for 60 min. The mixture was then filtered and the collected product was put in a hot water bath for 10 min. The collected samples were then processed to measure sugar concentration by standard DNS method and measured under UV-VIS spectrophotometer at 540nm wavelength.

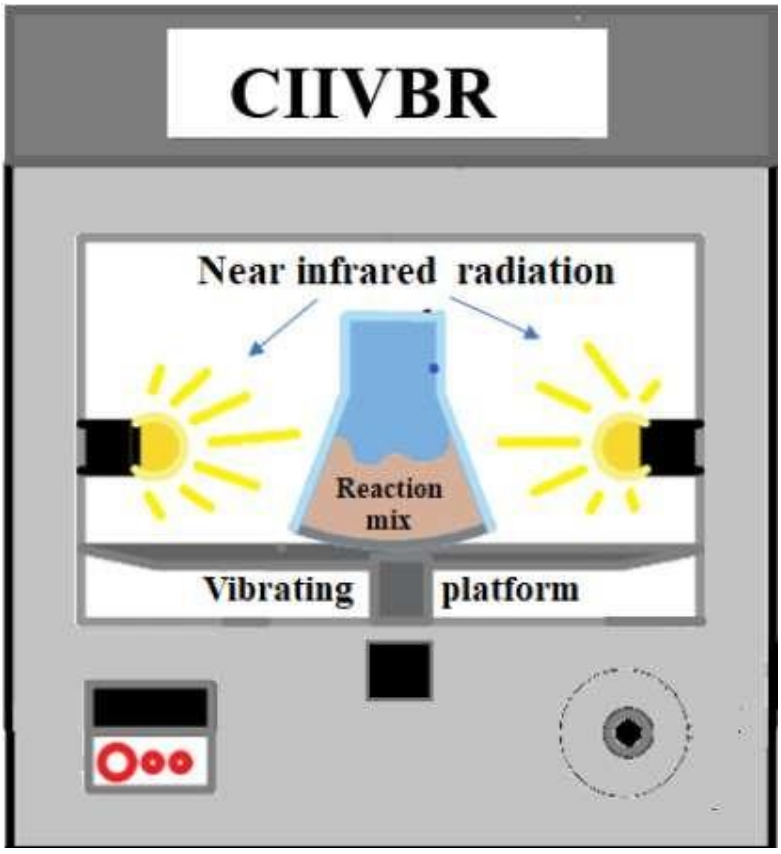


Fig.10 Model of CIIVBR

6.3.6 Saccharification of PWBP with CIMPI

1g peracetic acid treated banana pseudostem was mixed in a round bottle one neck flux with 20ml deionized water and 5ml acetic acid buffer solution. After that 1ml CIMPIwas added into the mixture and set in a carbon infrared irradiated vibrating batch reactor (CIIVBR) (100 W, 750–1400 nm) at 40° C for 60min. The liquid sample was then collected through filtration and heated at 60° C for 10 min to stop further reaction in the filtrate media. The biomass collected in the filter paper was separated and collected for further characterization. Varying reaction time, temperature, CIMPI concentration and biomass to water ratio nine solutions are prepared by following the using L9 Taguchi experimental design (L9TED).

Subsequently, the sample solutions are placed on CIIVBR for the particular reaction time given in the L9TED. The reaction mixture was then allowed to cool down to room temperature and then stored after being filtered through filtered paper and the product was analyzed via DNS treatment (Miller, 1959) and HPLC.



Fig.11 Ultrasonic Homogenizer



Fig.12 Magnetic property of CIMPI in presence of magnet



Fig.13 FS in presence of DNS

6.3.7 Experimental layout and process optimization using Taguchi design:

To analyze the effects of all independent process factors on the response factor [sugar yield], nine (9) experimental runs of the cellulose hydrolysis were conducted using TOAD ["MINITAB-19": Minitab Inc. USA for Windows10] (Table 3) with select process variables (Table 2). Through assessment of signal to noise (S/N) ratios and analysis of variance, it also assesses a set of optimal process variables corresponding to the maximum sugar yield

(ANOVA). Here, the signal (S) represented the response's arithmetic mean across three experimental replication values, while the noise (N) indicated the trial's respective standard deviation (Table 1). The response factor was also maximized utilizing the “larger is better” criterion.

$$\frac{S}{N} = -10\ log\ (\frac{1}{n}\sum_{i=1}^{n}\frac{1}{\theta_{FS,i}^{2}}) \ldots\ldots (2)$$

where, i stands for the number of replications, n for the number of experimental runs performed at a particular set condition, and Θ_S denotes response factor, Sugar yield.

Table.2 Independent process variables for saccharification of PWBP with CIMPI

Process variables	Temperature (°C)	Time (min)	PWBP : Water (w/w)	CIMPI (wt.%)
L_1	30	40	3	1.5
L_2	40	60	4	2.5
L_3	50	80	5	3.5

6.3.8 UV-vis spectroscopyanalyses of pretreated waste banana pseudostem saccharified substance (PWBPSS)

After hydrolysis, DNS reagent (0.5 mL) and saccharified substance sample (0.5 mL) were mixed with deionized water (0.5 mL) that was kept at 100 °C for 5 min and then allowed to cool at room temperature. The resultant mixture was diluted with 4 mL of deionized water to make the dilution factor 11 [0.5 (sample volume): 5.5 (total solution volume)], and the absorbance of the mixture was measured by a UV spectrophotometer at 540 nm.[14] UV-vis spectroscopy is an analytical technique that measures the number of discrete wavelengths of UV or visible light that are absorbed by or transmitted through a sample in comparison to a reference or blank sample. This property is influenced by the sample composition, potentially providing information on what is in the sample and at what concentration. Whichever wavelength selector is used in the spectrophotometer; the light then passes through a sample. For all analyses, measuring a reference sample, often referred to as the "blank sample", such as a cuvette filled with a similar solvent used to prepare the sample, is imperative. If an aqueous buffered solution containing the sample is used for measurements, then the aqueous buffered solution without the substance of interest is used as the reference. The FS yield was

calculated using a standard curve obtained with glucose. The mass of S (M_S) and the yield of sugar were using a standard curve obtained with glucose. (Figure 14).

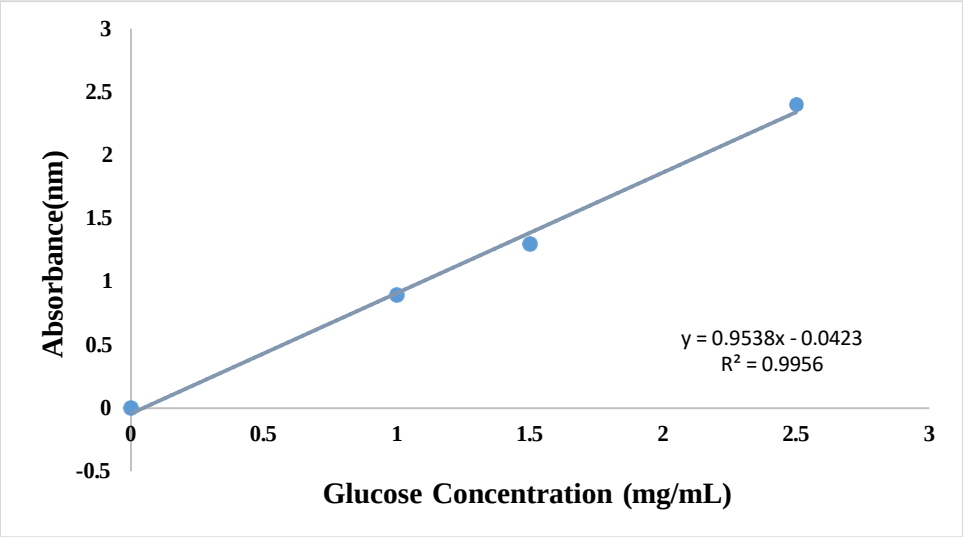


Fig.14 Standard curve of glucose at 540 nm

M_s(mg) = RS concentration(mg/ml) $\times VRM(ml) \times DF$

$$\text{FS Yield} = M_s \times \frac{MWG - MW}{MWG \times 100} \times 100 \ldots\ldots (3)$$

Where M_S is the mass of Sugar (mg); VRM is the volume of reaction mixture (mL); DF is the dilution factor = 11; MWG is the molecular weight of glucose (as a monomer of cellulose) =180.16; MWW is the molecular weight of water = 18.02. Sugar yield was determined by standard DNS method (Miller, G. L. 1959).

6.3.9 HPLC analyses of PWBPSS

After saccharification,the PWBPSS compositions were also quantified using high performance liquid chromatography (HPLC) with a refractive index detector (Perkin Elmer 200 Series) along with 300 × 7.8 mm Bio-Rad HPXP, 9 µm column at a flow rate of 0.6 mL min^{-1} of 0.005M of sulfuric acid (mobile phase). The concentration of the significant compounds in the saccharified substance was evaluated individually using a calibration plot developed by analyzing the respective standard compounds of identified concentrations.

6.3.10 Preparation of yeast mixture and bio-ethanol production from FS of PWBP

For bio-ethanol production after the optimized saccharification process 100 ml PWBP saccharified substance was fermented using dry yeast viz. *Saccharomyces cerevisiae*. Dry yeast (*Saccharomyces cerevisiae)* was kept in luke-warm water for 3 min then the saccharified substance solution was inoculated with 1% (wt. /v) of *Saccharomyces cerevisiae*. Prior to addition of inoculums the pH of saccharified substance was adjusted to 4.5 using acetate buffer solution. The mixture was fermented for 96 h at 35˚Cin a controlled temperature in absence of oxygen and constant agitation of 120 rpm in a batch fermenter. The samples in the fermenter were collected at 12 h intervals and centrifuged at 4 °C at 2000 rpm for 10 min. 0.45-µl filters were used to filter the supernatant and checked for FS analysis and measuring the yield of bio-ethanol using UV- spectroscopy at around 220 nm. The alcohol content was also measured according to standard procedures.[36] using an alcohol hydrometer with a V/V% (scale: 0-100, 1.0% accuracy, at 20°C), manufactured by Leimco, Mumbai, India. The fractional distillation was performed using a distillation column at 78˚Cand the purified bio-ethanol was collected in air tight container.



Fig.15 a) batch fermentation using S. cerevisiae, b) bio-ethanol purification using distillation setup

The calculation of the fermentation efficiency is as follows:

$$FE = \frac{Bioethanol\,produced}{TME_S} \times 100 \ldots\ldots (4)$$

Where FE is fermentation efficiency and TMEs is theoretical maximum ethanol yield from sugar

From 1.11 g glucose maximum 0.567 g theoretical bioethanol can be produced.

The calculation of alcohol by volume % (ABV %) is as follows:

$$\text{ABV \%} = (OG - FG) \times 131.25 \ldots \ldots (5)$$

Where, OG is the Initial Gravity of the sample mix, and FG is the Final Gravity

131.25 = The conversion factor for the relative density of alcohol and water.

6.3.11 Characterization tests of the prepared CIMPI

The interaction of the nanoparticles with UV-Visible light was analyzed by recording the absorbance spectra of the suspension across multiple wavelengths ranging from 200 to 800 nm using a dual beam UV-Visible spectrophotometer (UV-1800, Shimadzu, Japan). The crystallinity of the Fe_3O_4 magnetic nanoparticles was assessed through powder X-ray diffraction (XRD) using a PANalyticalX'Pert Pro, following the method described by Xu et al.[16]The scans were performed using Cu-Kα radiation (λ = 1.54060 Å) at 45 kV and 40 mA, spanning the 2θ range from 20° to 80° at a scanning speed of 1° min^{-1}.The thermo stability of the enzymatic-chemo-photocatalyst (CIMPI) was assessed using a Thermo gravimetric Analysis (TGA) test across a wide temperature range of 40-750°C, with a heating rate of 100°C/min. The surface morphology of the optimized cellulase-immobilized nanoparticles was examined using Scanning Electron Microscopy (SEM; JSM-6100, Jeol, Japan). Additionally, their elemental composition was analyzed through energy dispersive X-ray spectroscopy (EDX; Thermo Fisher Scientific, US) (Lu et al., 2018). Fourier Transform Infrared Spectroscopy (FT-IR) was employed to assess the functional group characterization and enzyme binding on iron particles. The analysis was conducted using a Thermo Nicolet 6700 spectroscope operating in attenuated total reflectance (ATR) mode, covering the mid-IR range from 4000 to 400 cm^{-1} wave numbers (Burgula et al., 2006). The UV-visible diffuse reflectance spectroscopy analysis of CIMPI was conducted using the JASCO spectrophotometer model V-670. Photoluminescence (PL) spectroscopy was carried out with a Raman spectrometer. The specific surface area of the chemo-bio catalystwas determined using the BET (Brunner–Emmett–Teller) method, employing the Quanta Chrome NOVA 4000e instrument. Additionally, the pore volume and pore size profile of the optimized CIMPI enzymatic-chemo photocatalyst were assessed utilizing the BJH (Barret, Joyner, Halenda) method.

SEM

SEM, an imaging technique renowned for its ability to capture detailed three-dimensional images of various samples, operates by directing a focused beam of high-energy electrons, typically emitted by an electron source like a tungsten filament or field emission gun, onto the sample's surface. Interactions between the electron beam and the atoms of the sample occur during scanning. These interactions lead to the emission of secondary electrons (SE) from the sample's surface, offering topographical insights crucial for generating SEM images. Additionally, backscattered electrons (BSE) are gathered, providing contrast in terms of composition and atomic number. These signals are then detected and processed to produce high-resolution three-dimensional images illustrating the surface morphology and composition of the sample.



Fig.16 SEM instrument

EDS mapping

Energy Dispersive X-ray Spectroscopy (EDS) is a technique commonly used in conjunction with Scanning Electron Microscopy (SEM) to analyze the elemental composition of a sample. In EDS, as the electron beam from the SEM interacts with the atoms in the sample, it can cause inner shell electrons to be ejected from the atoms. When this occurs, outer shell electrons transition to fill the vacancies left behind in the inner shells. As these outer shell electrons transition, they release energy in the form of characteristic X-rays. The energy of these X-rays is unique to each element, allowing for identification of the elements present in

the sample. EDS detectors collect and measure the energies of these X-rays. By analyzing the energy spectrum of the collected X-rays, EDS can provide information about the elemental composition of the sample.

TGA

TGA (Thermogravimetric Analysis) is a technique used in materials science and chemistry to study thermal stability and composition by measuring sample mass changes with controlled heating. Key steps include sample preparation, controlled heating in a defined atmosphere (e.g., air, nitrogen), continuous mass monitoring, and result interpretation based on mass changes against temperature or time. TGA helps determine thermal stability, decomposition temperatures, and composition changes in materials. It's used for assessing purity, identifying decomposition events, and measuring sample composition based on weight loss. Applications include quality control, process optimization, and material characterization in research and industry. Overall, TGA is vital for studying material properties like thermal stability and composition evolution under controlled conditions, aiding in diverse applications across science and industry.



Fig.17 TGA instrument

FTIR

Fourier Transform Infrared Spectroscopy (FTIR) is a powerful analytical technique used to identify chemical bonds and functional groups in a sample by measuring its infrared absorption spectrum. FTIR works by passing infrared radiation through a sample, which causes the molecules in the sample to vibrate at characteristic frequencies corresponding to

the bonds present. The interaction between the infrared radiation and the sample leads to absorption of specific wavelengths of light, resulting in dips (absorption bands) in the infrared spectrum. The intensity and position of these absorption bands provide information about the types of chemical bonds and functional groups present in the sample. By comparing the observed spectrum with reference spectra, FTIR can identify unknown substances or confirm the presence of specific functional groups within a sample.



Fig.18 FTIR instrument

XRD

X-ray Diffraction (XRD) is a technique used to analyze the crystal structure of materials. It operates by directing a beam of X-rays onto a sample, where they interact with the electron clouds surrounding the atoms. Some of these X-rays are scattered by the electrons in the sample, resulting in a diffraction pattern consisting of peaks at specific angles. These peaks correspond to the angles at which X-rays are diffracted by the crystal lattice planes within the sample. By analyzing the positions and intensities of these peaks, XRD provides valuable information about the crystal structure, lattice parameters, crystal orientation, and phase composition of the material, making it a vital tool in materials science, geology, chemistry, and other fields.



Fig.19 XRD instrument

BET

The Brunauer-Emmett-Teller (BET) method is a widely used technique for determining the specific surface area of porous materials, such as catalysts, adsorbents, and powders. BET operates on the principle of gas adsorption, typically using nitrogen as the adsorbate. In this method, a known quantity of gas is introduced to the sample at various pressures and temperatures. As the gas molecules interact with the surface of the sample, they form a monolayer of adsorbed molecules. By measuring the amount of gas adsorbed at different pressures, the BET equation calculates the surface area of the sample based on the assumption of multilayer adsorption onto a surface with uniform energy sites. The resulting surface area is expressed in terms of the monolayer coverage of the sample, providing valuable information about its porosity and surface properties.

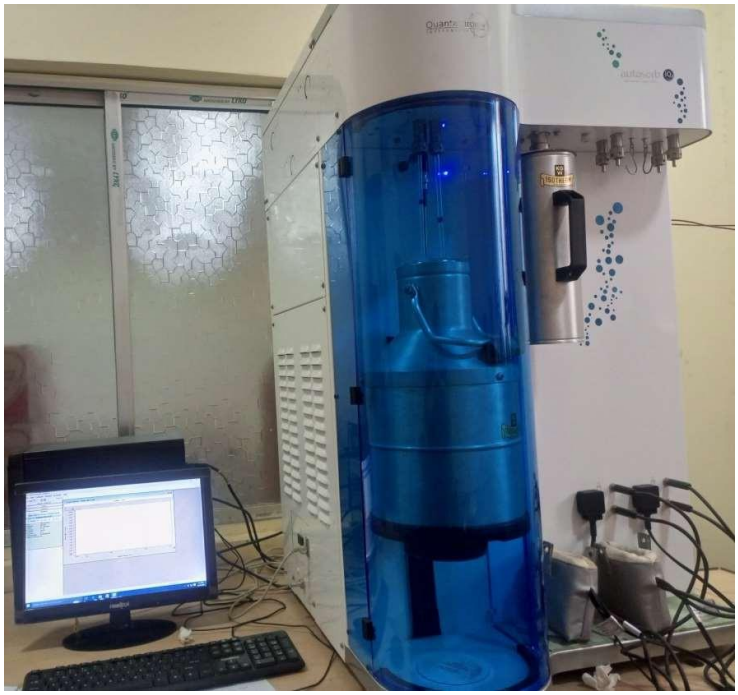


Fig.20 BET instrument

Taguchi orthogonal array

- Utilizing the Signal to Noise (S/N) ratio, Taguchi modeling proves highly effective in adjusting input parameters based on experimental outcomes or signals. The S/N ratio quantifies the ratio of meaningful data to experimental noise, thus highlighting the efficacy of optimization. Hence, experiments yielding higher S/N ratio values are deemed more ideal. The nature of the response dictates how the S/N ratio functions. The 'Larger the better' concept is employed when optimizing for a maximum response region, while the 'Smaller is better' concept is utilized for minimizing the optimal response. Employing the 'Nominal is best' formula seeks to attain an optimal response value, thereby enhancing data quality. In instances such as surface roughness, the 'Smaller is best' approach is preferred. A higher S/N ratio indicates reduced extraneous noise and enhanced signal relevance, ultimately leading to better optimized outcomes.

6.3.12 Product Characterization

High performance liquid chromatography (HPLC)-HPLC is a separation technique that involves:

- ✓ The injection of a small volume of liquid sample
- ✓ Into a tube packed with tiny particles (3to 5micron (µm)in diameter called the

stationary phase)

✓ Where individual components of the sample are moved down the packed tube (column) with a liquid (mobile phase) forced through the column by high pressure delivered by a pump.

✓ These components are separated from one another by the column packing that involves various chemical and/or physical interactions between their molecule sand the packing particles.

✓ These separated components are detected at the exit of this tube (column) by a flow-through device (detector) that measures their amount. An output from this detector is called a "liquid chromatogram".

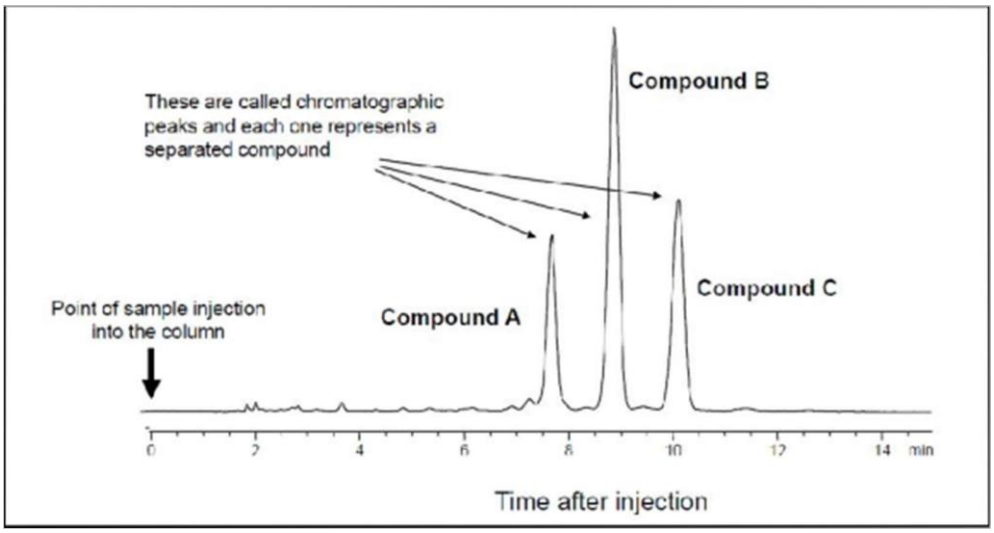


Fig.21 Example of a chromatogram

5 major Components of HPLC:

✓ Pump: The role of the pump is to force a liquid (called the mobile phase) through the liquid chromatography at a specific flow rate, expressed in milliliters per min (mL/min).

✓ Injector: The injector serves to introduce the liquid sample into the flow stream of the mobile phase.

✓ Column: Considered the "heart of the chromatograph" the column's stationary phase separates the sample components of interest using various physical and chemical parameters.

✓ Detector: The detector can detect the individual molecules that come out (elute) from the column.

✓ Computer: Frequently called the data system, the computer not only controls all the modules of the HPLC instrument but it takes the signal from the detector and uses it to determine the time of elution (retention time) of the sample components (qualitative analysis) and the amount of sample (quantitative analysis).

A part of the proposed research work deals with cellulose saccharification using cellulase-magnetic enzyme. The cellulose saccharification process is monitored using HPLC. A simple and reproducible HPLC with refractive index (RI) detector is used for qualitative and quantitative analysis of sugars (glucose) in the sample.

Spectrophotometer

A spectrophotometer is employed to measure the amount of light that a sample absorbs. The instrument operates by passing a beam of light through a sample and measuring the intensity of light reaching a detector. In UV spectroscopy the light of ultra-violet region (200-400 nm.) is absorbed by the molecule. Absorption of the ultra-violet radiations results in the excitation of the electrons from the ground state to higher energy state. The energy of the ultra-violet radiation that is absorbed is equal to the energy difference between the ground state and higher energy states.

UV spectroscopy obeys the Beer-Lambert law, which states that: when a beam of monochromatic light is passed through a solution of an absorbing substance, the rate of decrease of intensity of radiation with thickness of the absorbing solution is proportional to the incident radiation as well as the concentration of the solution.

The expression of Beer-Lambert law is:

$$A = log_{10}(\frac{I^{\circ}}{I}) = scL$$

Where A is the measured absorbance, in Absorbance Units (AU), I^0 is the intensity of the incident light at a given wavelength, $I$is the transmitted intensity, L the path length through the sample, and c the concentration of the absorbing species. For each species and wavelength, ε is a constant known as the molar absorptive or extinction coefficient.

Though other techniques are available but spectrophotometer is widely applied for its

simplicity, versatility, speed, accuracy and cost-effectiveness. In the above mentioned work plan, UV-Vis spectrophotometer will be used for quantitative analysis of glucose concentration and protein concentration respectively. While fermentation of glucose is being carried using various yeast strains, samples will be collected at regular intervals for analysis of remaining glucose by spectrophotometer.

Spectrophotometric method for protein analysis: The **Bradford protein assay** is a spectroscopic analytical procedure used to measure the concentration of protein in a solution. It is subjective, i.e., dependent on the amino acid composition of the measured protein. The Brad ford assay, a colorimetric protein assay, is based on an absorbance shift of the dye Coomassie Brilliant Blue G-250 in which under acidic conditions the red form of the dye is converted in to its bluer form to bind to the protein being assayed. The (bound) form of the dye has an absorption spectrum maximum historically held to beat 595 nm. The cationic (unbound) forms are green or red. The binding of the dye to the protein stabilizes the blue anionic form. The increase of absorbance at 595 nm is proportional to the amount of bound dye, and thus to the amount (concentration) of protein present in the sample.

Spectrophotometric method for glucose analysis: 3, 5-Dinitrosalicylic acid (DNSA) is used extensively in biochemistry for the estimation of fermentable sugars. It detects the presence of free carbonyl group (C=O) of fermentable sugars. This involves the oxidation of the aldehyde functional group (in glucose) and the ketone functional group (in fructose). During this reaction DNSA is reduced to 3- amino-5-nitrosalicylic acid (ANSA) which under alkaline conditions is converted to a reddish brown coloured complex which has an absorbance maximum of 540 nm.

6.3.13 Life cycle analysis (LCA) study

The study conducted an analysis of the overall sustainability of the bio-ethanol synthesis process from pretreated banana pseudostem using CIMPI, employing the openLCA software with ecoinvent database 3.7 and LCA process “ReCiPe Midpoint (H)”for Life Cycle Assessment (LCA). Furthermore, it delved into the environmental impacts associated with the reusability of the prepared CIMPI compared to fresh CIMPI to gauge the effectiveness of the optimal biocatalyst in FS synthesis. The investigation utilized a gate-to-gate LCA approach, wherein the first system boundary covered the transport of chemicals and the preparation of CIMPI, while the second system boundary encompassed the pretreatment of waste banana pseudostem, the synthesis process of FS from PWBP using CIMPI, and

ultimately, the fermentation of FS to bio-ethanol, adopting a gate-to-grave perspective (Fig.22).A Life Cycle Inventory (LCI) database was developed according to the system boundary, with inputs and outputs of the entire process scaled-up based on the functional unit (1 kg bio-ethanol). The detailed LCI database is provided in the supplementary document (Table 3-7). The environmental impacts, including acidification, eutrophication, photochemical ozone formation, Global Warming Potential (GWP), and land use, were assessed using the "ReCiPe Midpoint (H)" LCA methodology, utilizing the ecoinvent database 3.7 (Roy Choudhury et al.,2023).

Table 3. LCI database for 1 Kg PWBP preparation

Category	Flow	Value	Unit	Source	Comments
Energy Input	Electricity consumed	2.12	kWh	Ecoinvent 3.7	
Material Input	Waste banana pseudostem	1.34	Kg	Ecoinvent 3.7	
	H_2O_2	0.75	Kg	Ecoinvent 3.7	
	Acetic acid	2.54	Kg	Ecoinvent 3.7	
Transports	Waste banana pseudostem	0.011	Kg.km	Ecoinvent 3.7	Transport by lorry, capacity: 18 metric ton, EURO
	H_2O_2	0.0043	Kg.km	Ecoinvent 3.7	
	Acetic acid	0.0117	Kg.km	Ecoinvent 3.7	
	Total	**0.027**	**Kg.km**	Ecoinvent 3.7	VI (assuming all materials came from 100 km distance)
Emissions to air	Waste heat	6.41	MJ	Ecoinvent 3.7	Assuming electrical energy used was dissipated as heat to air (1 kWh =3.6 MJ)
Output	**PWBP**	**1**	**Kg**	**Created**	

Table 4. LCI database for 1 Kg of optimal CIMPI preparation

Category	Flow	Value	Unit	Source	Comments
Energy Input	Electricity consumed	0.083	kWh	Ecoinvent 3.7	

Material Input	Fe_3O_4	0.149	Kg	Ecoinvent 3.7	
	Cellulase Enzyme	0.093	Kg	Ecoinvent 3.7	
	Glutaraldehyde	0.101	Kg	Ecoinvent 3.7	
	APTES	0.201	Kg	Ecoinvent 3.7	
Transports	Fe_3O_4	0.00201	Kg.km	Ecoinvent 3.7	Transport by lorry, capacity: 16 metric ton, EURO VI (assuming all materials came from 100 km distance)
	Cellulase Enzyme	0.00102	Kg.km	Ecoinvent 3.7	
	Glutaraldehyde	0.00156	Kg.km	Ecoinvent 3.7	
	APTES	0.00149	Kg.km	Ecoinvent 3.7	
	Total	**0.00608**	**Kg.km**	Ecoinvent 3.7	
Emissions to air	Waste heat	0.1583	MJ	Ecoinvent 3.7	Assuming electrical energy used was dissipated as heat to air (1 kWh =3.6 MJ)
Emissions to water bodies	Waste water	0.6	L	Ecoinvent 3.7	Assuming impure water had undergone waste water treatment
Output	**CIMPI**	**1**	**Kg**	**Created**	

Table 5. LCI database for 1 Kg FS production in CIIVBR

Category	Flow	Value	Unit	Source	Comments
Energy Input	Electricity consumed	0.23	kWh	Ecoinvent 3.7	
Material Input	PWBP	1.567	Kg	Ecoinvent 3.7	
	CIMPI	0.357	Kg	Ecoinvent 3.7	
	Water	0	Kg	Ecoinvent 3.7	(As CIMPI was recovered and recycled)
Transports	Water	0.0108	Kg.km	Ecoinvent 3.7	
Emissions to air	Waste heat	1.21	MJ	Ecoinvent 3.7	Assuming electrical energy used was dissipated as heat to air (1 kWh =3.6 MJ)
Emission to water bodies	Waste water	1.2	L	Ecoinvent 3.7	Assuming the impure water underwent wastewater treatment.
Output	FS	1	Kg	Created	

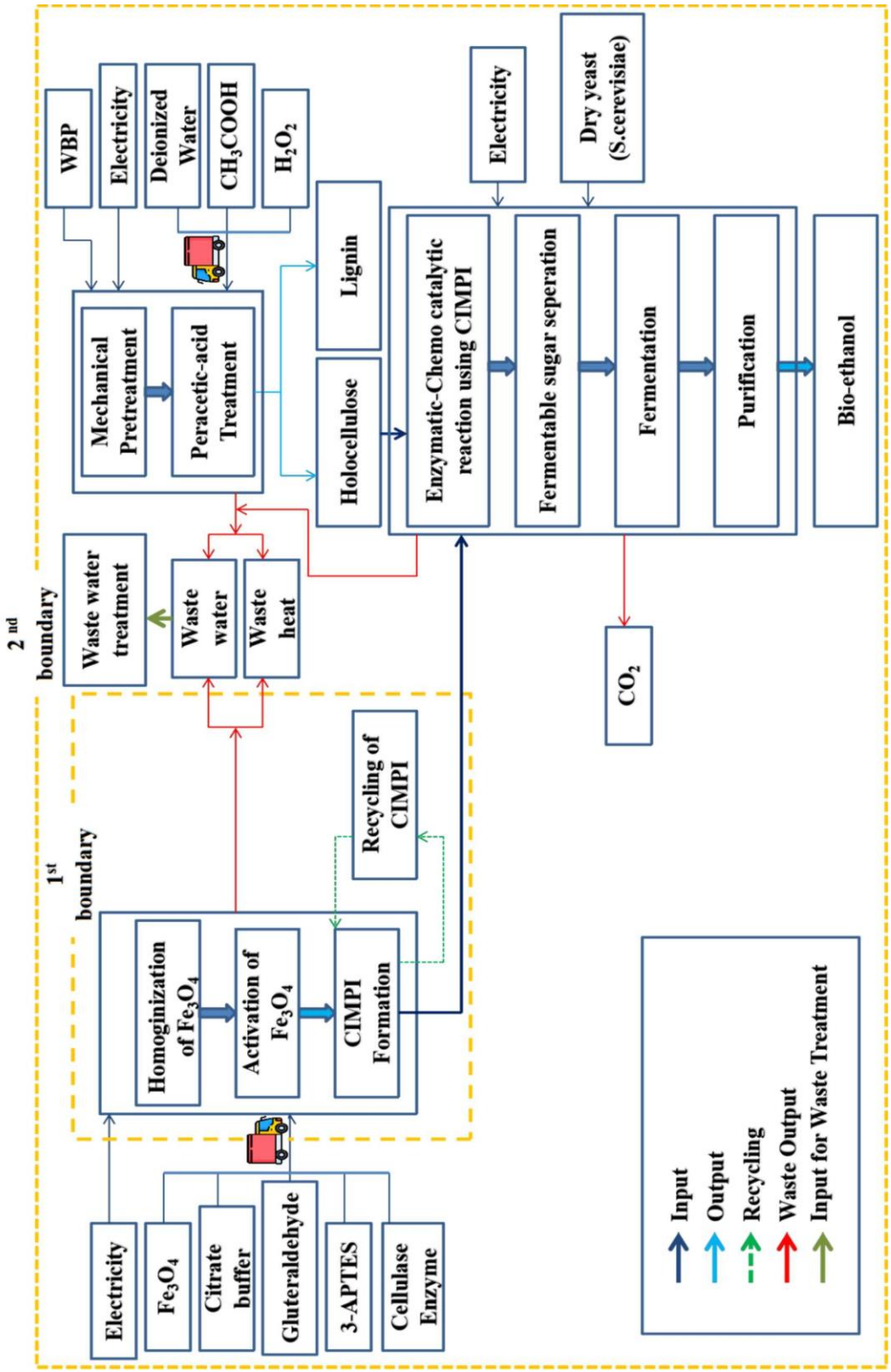
Table 6. LCI database for 1 Kg FS production in CBR

Category	Flow	Value	Unit	Source	Comments
Energy Input	Electricity consumed	0.45	kWh	Ecoinvent 3.7	
Material Input	PWBP CIMPI Water	1.567 0.357 0.5	Kg Kg Kg	Ecoinvent 3.7 Ecoinvent 3.7 Ecoinvent 3.7	(As CIMPI was recovered and recycled)
Transports	Water	0.0108	Kg.km	Ecoinvent 3.7	
Emissions to air	Waste heat	2.13	MJ	Ecoinvent 3.7	Assuming electrical energy used was dissipated as heat to air (1 kWh =3.6 MJ)
Emission to water bodies	Waste water	1.8	L	Ecoinvent 3.7	Assuming the impure water underwent wastewater treatment.
Output	FS	1	Kg	Created	

Table 7. LCI database for 1 Kg Bio-ethanol production

Category	Flow	Value	Unit	Source	Comments
Energy Input	Electricity consumed	0.31	kWh	Ecoinvent 3.7	
Material Input	FS Dry Yeast Water	1 0.5 2.5	Kg Kg Kg	Created Ecoinvent 3.7 Ecoinvent 3.7	
Transports	Water	0	Kg.km		
Emissions to air	Waste heat	0.7675	MJ	Ecoinvent 3.7	Assuming electrical energy used was dissipated as heat to air (1 kWh =3.6 MJ)
Output	Bio-ethanol	1	Kg	Created	

Fig.22 LCA boundary system



6.4 Methods for production of FS from PL

6.4.1 Physical pretreatment of pineapple leaves

Pineapple leaves (PL) was collected and washed with deionised water thoroughly. It was cut evenly and then air dried in a hot air oven at 90° C for 4h. The dried biomass was then ground in a grinder and mechanical sieving was done to obtain biomass in a particle range of around 300 mesh size. For an effective delignification process modified infrared irradiated peracetic acid treatment was done. (Roy Choudhuryet al. 2021)

.

6.4.2 Chemical pretreatment of waste banana pseudo-stem

At first 10 g of sieved PL was weighed and 10 ml of peracetic acid was mixed in a one-neck round bottle flux. 60 ml of glacial acetic acid was then transferred into the mixture. The mixture was then reacted in CIIVBR (100 W, 750–1400 nm) at 90° C for 150 min maintaining a speed of 800-900 rpm. Vacuum filtration was conducted to separate the biomass and a hot water wash was done to remove peracetic acid. The separated lignin was collected for further quantification. The filtrate was oven-dried at 80 °C to get the dried biomass. The anthrone approach (Table.8) was utilised to conduct a compositional analysis of the WBP and PWBP.

Table.8 Compositional analysis of WBP and PWBP

Compositional analysis*	PL (wt. %)	PPL (wt. %)
Cellulose	76	74.5
Hemicellulose	17	15.1
Lignin	5	1.76
Others	2	0.02

* Compositional analysis was done based on Anthrone method [Ludwig et al. 1956]

6.4.3 Cellulase immobilization on magnetic photo-active iron particles

At first tin-cloride particles were calcined at 800°C for 150min then it was cooled and washed with 0.1M citrate buffer solution and sonicated in an ultrasonic homogenizer (TAKASHI- U250) for 10 minutes to disperse particles homogeneously. Then the tin oxide particles were collected using a magnet. 7 ml of 1M glutaraldehyde solution was added and

incubated in acarbon infrared irradiated vibrating batch reactor (CIIVBR) (100 W, 750–1400 nm) at 37° C for 1h at 120 rpm for activation of tin oxide particles. The activated particles were collected with a magnet and washed with 0.1M carbon infrared irradiated vibrating batch reactor citric acid buffer solution to remove excess glutaraldehyde from the mixture. Then the cellulase enzyme suspended in 0.1M citrate buffer was mixed with 3-APTES and incubated with activated magnetic particles at 37° Cfor 20h. The cellulase immobilized photoactive tin (CIPSn) was collected with a magnet and washed with buffer solution which was then centrifuged at 4°Cfor 15mins at 4000rpm.The unbound enzyme was separated and the immobilized enzymatic-chemo catalyst was further vacuum dried for complete drying of the sample. The CIMPI was stored under refrigerated conditions for further application and characterization.

6.4.4 Saccharification of PL with CIPSn

1g peracetic acid treated PL was mixed in a round bottle one neck flux with 20ml deionized water and 5ml acetic acid buffer solution. After that 1ml CIPSn was added into the mixture and set in a carbon infrared irradiated vibrating batch reactor (CIIVBR) (100 W, 750–1400 nm) at 40° C for 60min. The liquid sample was then collected through filtration and heated at 60° C for 10 min to stop further reaction in the filtrate media. The biomass collected in the filter paper was separated and collected for further characterization. Varying reaction time, temperature, CIPSn concentration and biomass to water ratio nine solutions are prepared by following the using L9 Taguchi experimental design (L9TED).

Subsequently, the sample solutions are placed on CIIVBR for the particular reaction time given in the L9TED. The reaction mixture was then allowed to cool down to room temperature and then stored after being filtered through filtered paper and the product was analyzed via DNS treatment (Miller, 1959) and HPLC.

6.4.5 Experimental process optimization using Taguchi design:

Table.9 Independent process variables for saccharification of PL with CIPSn

Process variables	Temperature (°C)	Time (min)	PL: CIPSn
L_1	40	45	10 : 1
L_2	60	65	10 : 2
L_3	80	85	10 : 3

6.4.6 UV-vis spectroscopy analyses of pretreated PL saccharified substance (PPLSS)

After hydrolysis, DNS reagent (0.5 mL) and saccharified substance sample (0.5 mL) were mixed with deionized water (0.5 mL) that was kept at 100 °C for 5 min and then allowed to cool at room temperature. The resultant mixture was diluted with 4 mL of deionized water to make the dilution factor 11 [0.5 (sample volume): 5.5 (total solution volume)], and the absorbance of the mixture was measured by a UV spectrophotometer at 540 nm.[14] UV-vis spectroscopy is an analytical technique that measures the number of discrete wavelengths of UV or visible light that are absorbed by or transmitted through a sample in comparison to a reference or blank sample. This property is influenced by the sample composition, potentially providing information on what is in the sample and at what concentration. Whichever wavelength selector is used in the spectrophotometer; the light then passes through a sample. For all analyses, measuring a reference sample, often referred to as the "blank sample", such as a cuvette filled with a similar solvent used to prepare the sample, is imperative. If an aqueous buffered solution containing the sample is used for measurements, then the aqueous buffered solution without the substance of interest is used as the reference.



Fig.23 DNS samples using L9TED

6.4.7 Characterization tests of the prepared CIPSn

The interaction of the nanoparticles with UV-Visible light was analyzed by recording the absorbance spectra of the suspension across multiple wavelengths ranging from 200 to 800 nm using a dual beam UV-Visible spectrophotometer (UV-1800, Shimadzu, Japan). The crystallinity of the SnO_2 photoactive particles was assessed through powder X-ray diffraction (XRD) using a PANalyticalX'Pert Pro, following the method described by Xu et al. The scans were performed using Cu-Kα radiation (λ = 1.54060 Å) at 45 kV and 40 mA, spanning the 2θ range from 20° to 80° at a scanning speed of 1° min^{-1}.The thermo stability of the enzymatic-chemo-photocatalyst (CIPSn) was assessed using a Thermo gravimetric Analysis (TGA) test across a wide temperature range of 40-800°C, with a heating rate of 100°C/min. The surface morphology of the optimized cellulase-immobilized nanoparticles was examined using Scanning Electron Microscopy (SEM; JSM-6100, Jeol, Japan). Additionally, Fourier Transform Infrared Spectroscopy (FT-IR) was employed to assess the functional group characterization and enzyme binding on tin particles. The analysis was conducted using a Thermo Nicolet 6700 spectroscope operating in attenuated total reflectance (ATR) mode, covering the mid-IR range from 4000 to 400 cm^{-1} wave numbers (Burgula et al., 2006). The UV-visible diffuse reflectance spectroscopy analysis of CIPSn was conducted using the JASCO spectrophotometer model V-670.

CHAPTER 7

RESULTS & DISCUSSION

7.1 Results and discussion for WBP to Bio-ethanol conversion using CIMPI

7.1.1 WBP and PWBP composition analysis

To determine the sample's holo-cellulose and lignin content, the chemical composition of WBP and PWBP were measured. According to the preliminary analysis, the weight percentage composition of the WBP in this study is 50.43 wt.% cellulose, 29.28 wt.% hemicellulose, 17.86 wt.% lignin, and 2.43 wt.% others. The physical pretreatment of WBP made it expedient for the chemical pretreatment with peracetic acid. After treatment with peracetic acid under carbon irradiation in CIIVBR 16.1 wt.% of isolated lignin (purity 90.5%) could be attained.

7.1.2 FS yield analysis via UV Spectroscopy

By analyzing the graph (Table.1), the correlation between UV absorbance at 540nm and glucose concentration in mg/ml was determined. Subsequently, employing the eqs 3, the yield of FS was calculated to be 73.40%.

7.1.3 FS yield analysis via HPLC

HPLC was employed to assess the quantitative compositions of products obtained through optimal WBP pretreatment followed by the chemo-bio-conversion of PWBP in CIIVBR (Figure 24). The retention times for glucose, fructose, sucrose and HMF were determined to be 5.807, 6.088, 9.54, and 14.89 respectively, aligning well with findings by Namchot et al. Notably, the glucose concentration (65.51 mol%) was higher compared to the concentrations of fructose (47.07 mol%) sucrose (45 mol%), and HMF (18.9 mol %).

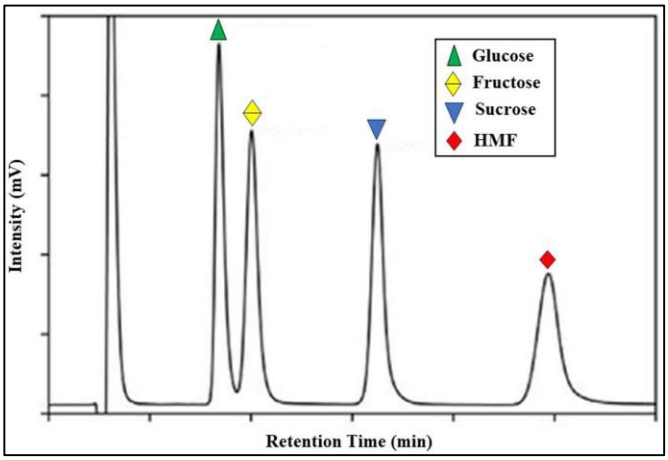


Fig. 24 HPLC of saccharified substance from PWBP using CIMPI chemo-biocatalyst under CIIVBR

7.1.4 Optimization of FS yield

Table 10. Representing 9 experimental runs as per L9TED

Temperature (^{0}C)	Time (min)	Biomass: Water (w/w)	CIMPI (wt.%)	Θ_{FS} (Sugar yield) (%)	SD	S/N ratio
30	40	3	1.5	52.69	±.18	31.48
30	60	4	2.5	57.48	±.07	36.24
30	80	5	3.5	58.76	±.14	37.73
40	40	4	3.5	62.46	±.24	40.08
40	60	5	1.5	50.52	±.03	37.94
40	80	3	2.5	62.38	±.11	36.27
50	40	5	2.5	65.41	±.15	38.67
50	60	3	3.5	73.40	±.03	45.16
50	80	4	1.5	65.76	±.12	35.76

Taking 9 runs designed from Taguchi optimization method, maximum sugar yield of 73.40 % can be achieved in the subsequent hydrolysis process at 60 min, 50 °C temperature with 3 biomass and water ratio and 3.5 CIMPI wt.%.

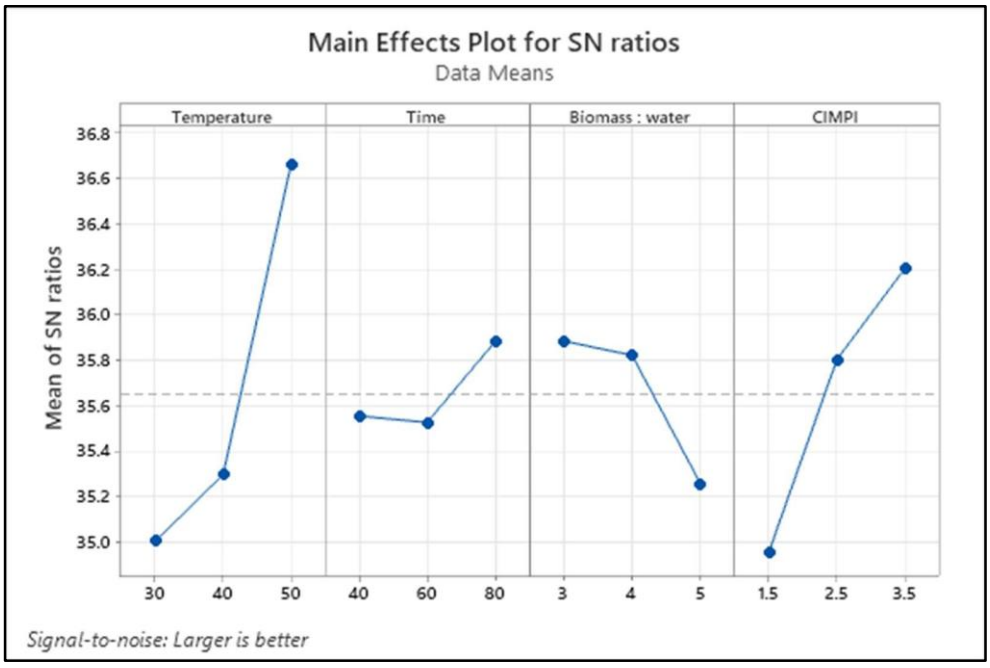


Fig. 25 Main effect plot for SN ratio

7.1.5 Characterization of WBP, PWBP and PWBPSS

XRD analyses

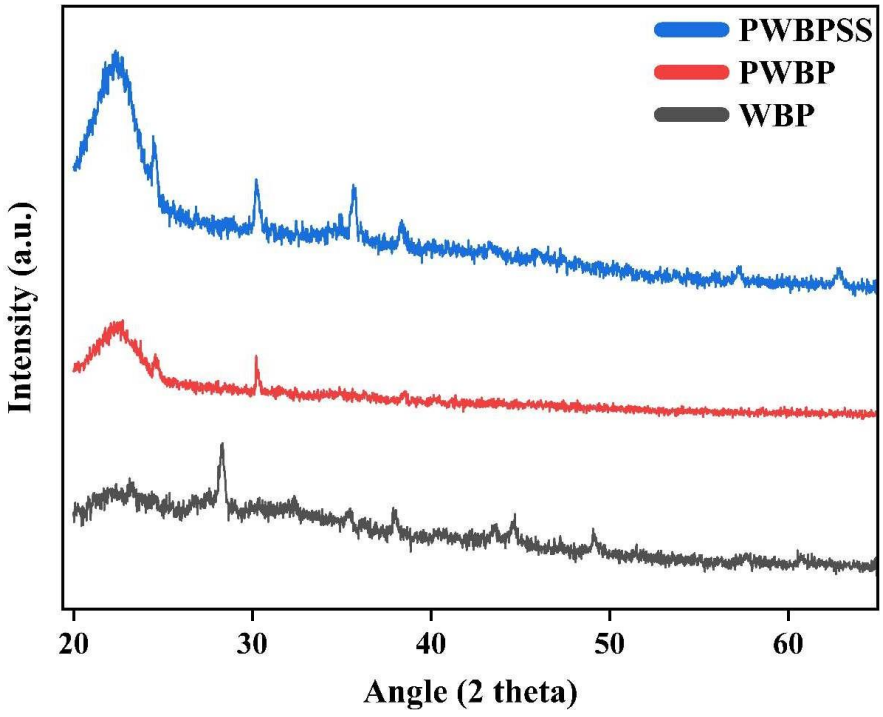


Fig.26 XRD pattern of PWBPSS, PWBP, WBP

XRD analysis was done for WBP, PWBP and PWBP saccharified substance (PWBPSS) obtained at optimal conditions to detect the crystal structure of cellulose by shining X-rays onto those samples and measuring the angles and intensities of the X-rays that are scattered by the sample's atomic planes. The analysis was done at 2Θ angle ranging from 20˚to 75˚with a scanning speed of 1° per minute using a Cu Kα source and an Intel CPS 120 hemispherical detector manufactured by Rigaku Miniflex Co. in Japan. In Figure 26 at 2Θ = 22.58° amorphous phases and crystalline structure of cellulose can be seen. Due to the gradual weakening of amorphous phases resulting from the pretreatment and saccharification processes, the intensity peak gradually sharpens.

7.1.6 Characterization of the prepared optimal chemo-biocatalyst (CIMPI)

I. SEM Analyses

Figure 27 displays the SEM image of Fe_3O_4 particles at 10KX and 50KX. To find the particle size, many particles were examined by ImageJ software. It is evident that the sample is made up of almost spherical, evenly distributed particles. The approximate value of particle size is around 182 nm.

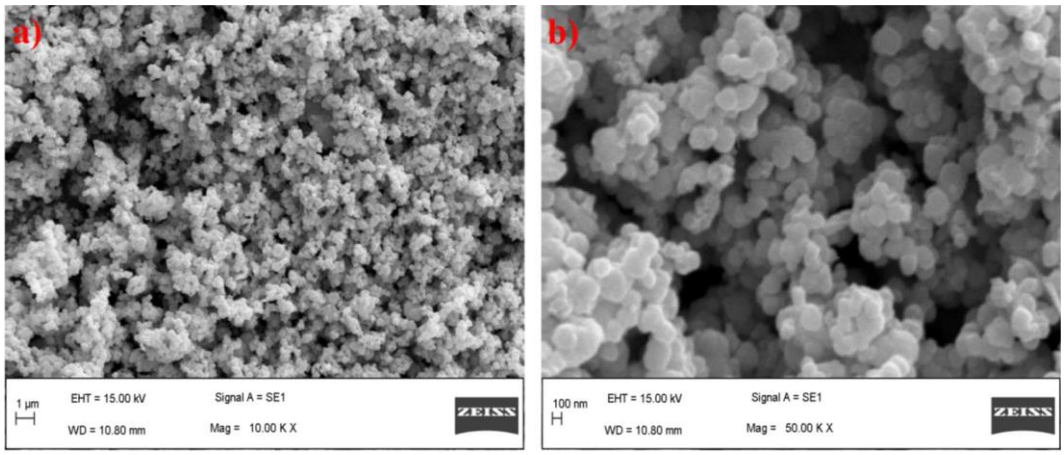


Fig.27 SEM images of iron oxide particles at a) 10000x and b) 50000x magnification

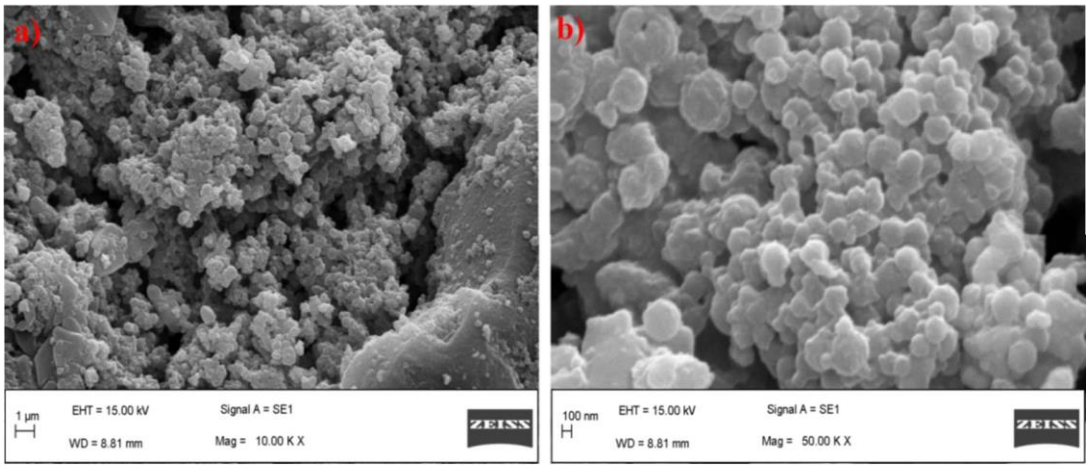


Fig.28 SEM images of CIMPI under a) 10000x and b) 50000x magnification

Due to magnetic dipole moments within the particles, the enzymes were aggregated, monodispersed, and had spherical shape with a smooth surface (Figure 28). A grain size around 240 nm was calculated using ImageJ software. Muley et al. reported that after APTES adding and enzyme immobilization on their surface, the shape of iron oxide magnetic particles remained almost spherical.

II. EDAX Analyses

EDAX analysis and mapping were doneto determine the percentage of each element present in the magnetic-photoactive immobilized enzyme with optimum performance. For analysis, a platinum coating was done. Elemental mapping was done for Fe_3O_4photoactive particles where non-uniform dispersion of oxygen and iron can be observed in 39% and 47% respectively in Figure 29, while EDAX of Fe_3O_4 in Figure 30 showed 16.6% oxygen and 72.5% iron present in the particles.

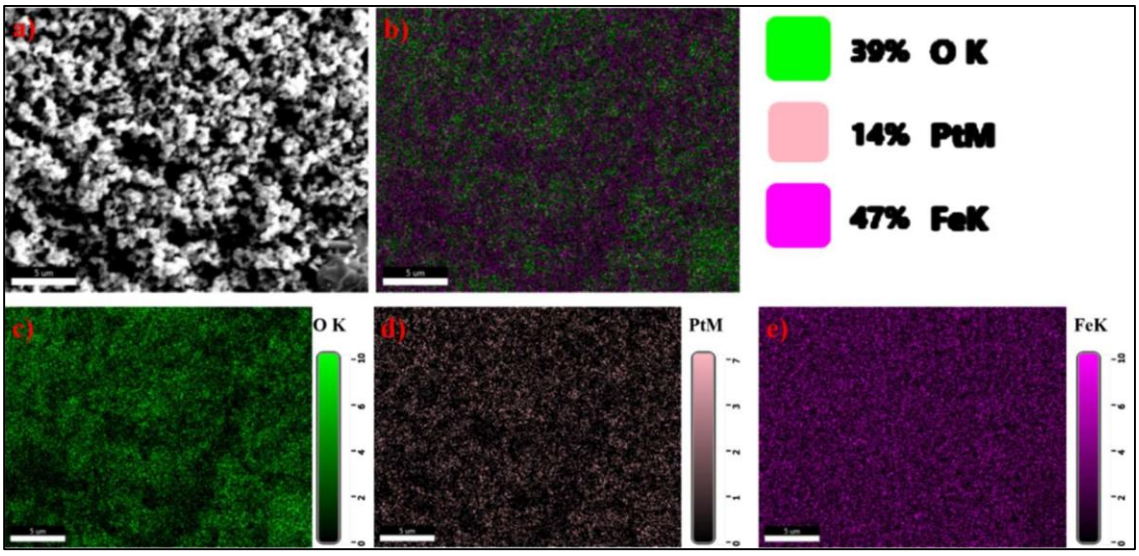


Fig.29 Elemental mapping of Fe_3O_4

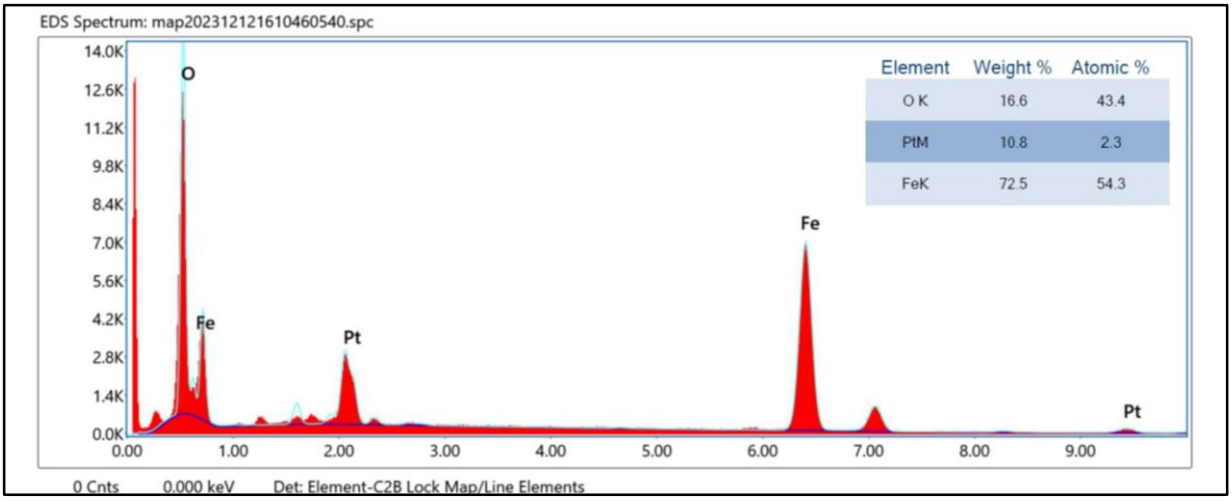


Fig.30 EDAX of Fe_3O_4 particle

Figure 31 shows theelemental mapping of cellulase immobilized magnetic-photo-active particles where non-uniform dispersion of Carbon, Nitrogen, Oxygen and Iron is observed in 38%, 4%, 33% and 5%. A platinum base was used. The EDAX of CIMPI (Figure 32) shows that the elements Carbon, Nitrogen, Oxygen and Iron present in the sample are 37.8%, 4.4%, 32.6%, 8.6%.

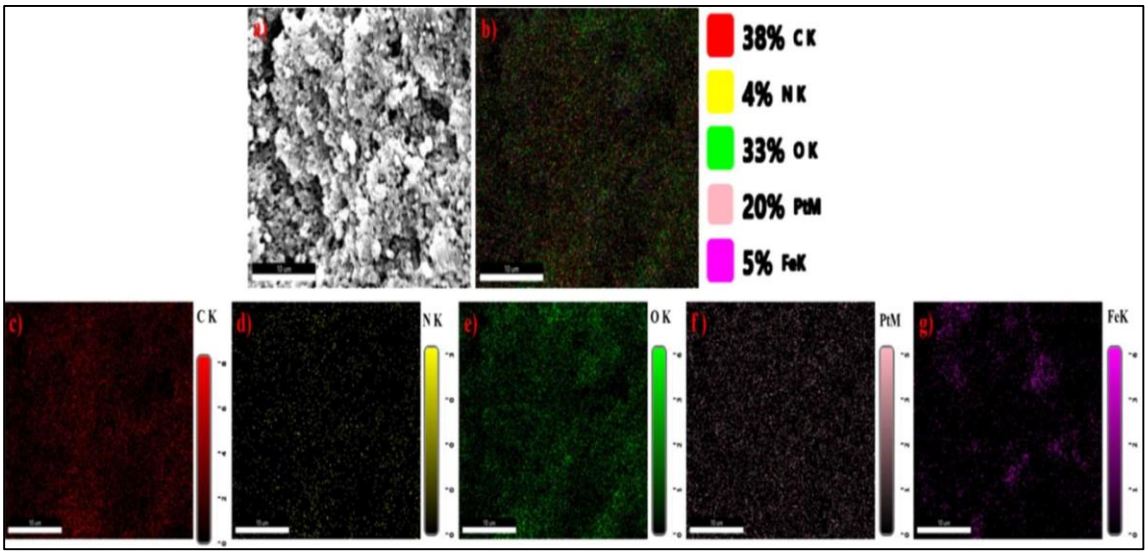


Fig.31 Elemental mapping of CIMPI

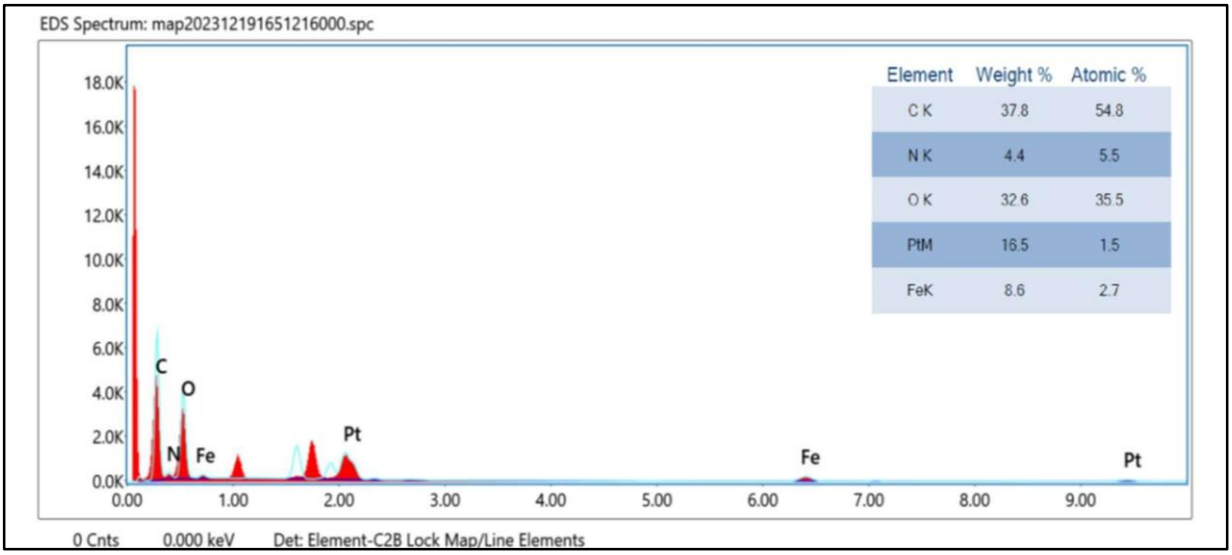


Fig.32 EDAX of CIMPI

III. XRD Analysis

XRD analysis of CIMPI was done to detect the crystal structure of cellulose and iron by shining X-rays onto those samples and measuring the angles and intensities of the X-rays that are scattered by the sample's atomic planes. The analysis was done at 2Θ angle ranging from 20°to 75° with a scanning speed of 1° per minute using a Cu Kα source and an Intel CPS 120 hemispherical detector manufactured by Rigaku Miniflex Co. in Japan. In Fig.33(a) at 2Θ = 30.29°, 35.74°, 37.16°, 46.72°, 53.73°, 57.30°, 62.82° crystalline peak of iron oxide (II, III)

can be seen and at 2Θ = 24.32°, 27.65°, 40.33°, 45.28°, 55.12°, 58.92° crystalline peak of Si can be seen due to the presence of Si in APTES.

IV. TGA Analysis

TGA patterns of CIMPI were done to assess the thermal stability of the prepared optimal CIMPI at different stages during heating over a vast range of 40-750 °C at 10 °C/min heating rate. In Figure 33(b) a weight loss of around 10% can be seen before 100 °C which is due to the release of unbound moisture from CIMPI. From temperature 100-300 °C a significant weight loss of 10% can be observed due to the release of unbound moisture from the CIMPI sample. After 300 °C temperature there is a steady fall can be observed in the TGA plot till 500 °C which is due to the combustion of cellulase and other organic substances. After 500 °C again a weight loss can be seen due to the slow combustion of iron oxide particles in CIMPI.

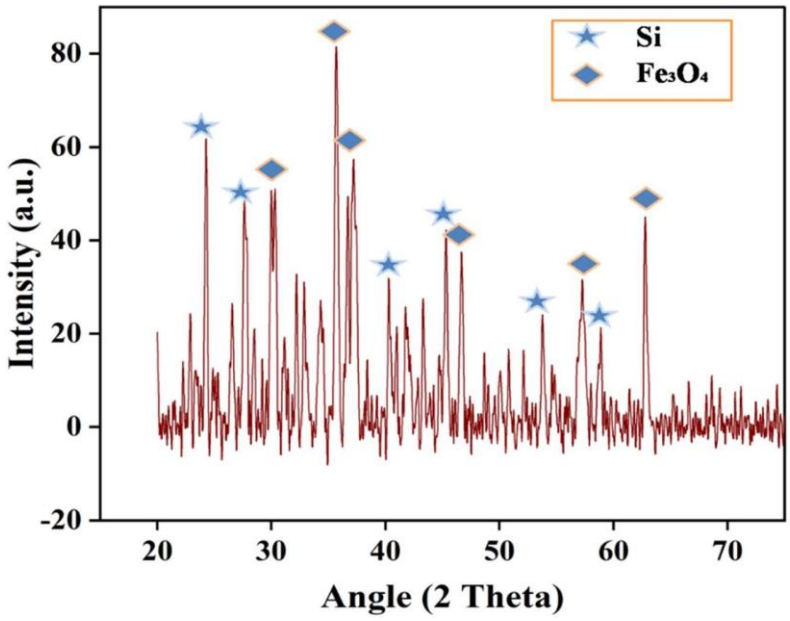
V. FTIR Analysis

FTIR of the CIMPI was done using PerkinElmer Spectrum. The N–H and O–H stretching vibrations were evident at 3445.71 cm^{-1}, while the C–H stretching vibration was observed at 2927.17 cm^{-1} in Figure 33(c). The characteristic peak at 619.72 cm^{-1} was attributed to Fe–O vibrations associated with MPs. Notably, the bands at 1593.27, 1388.42, and 1279.33 cm^{-1} corresponded to specific cellulase characteristics, indicating the binding of cellulase onto Fe_3O_4 particles. Furthermore, the appearance of a peak within the range of 1200–900 cm^{-1} confirmed the presence of Si–O–Si vibrations following APTES binding treatment on the CIMPI.

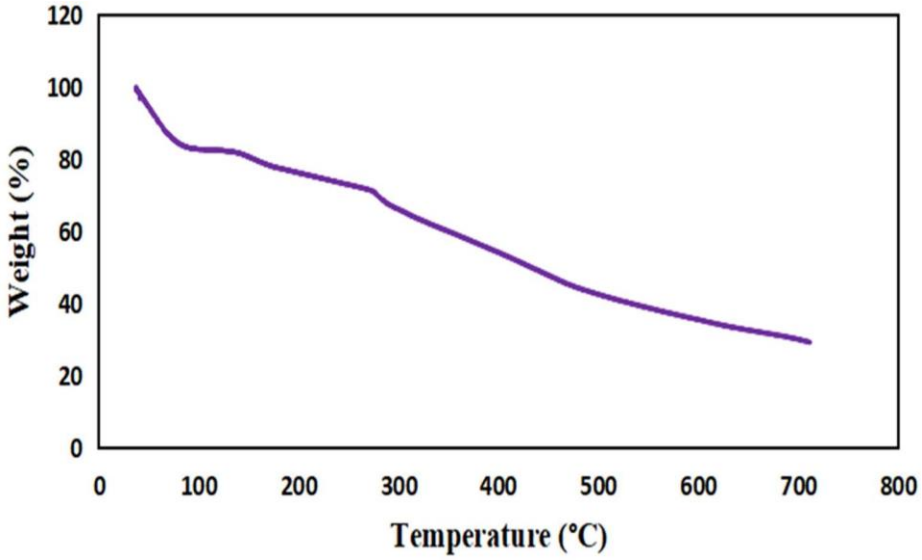
VI. UV-vis DRS analysis

Figure 33(d) presents the UV-Vis plot and the Tauc plot for bandgap analysis of CIMPI. Absorption spectroscopy analysis was performed on the synthesized magnetic photo-particles for light wavelengths ranging from 190 to 800 nm. The UV-Vis spectrum revealed a broad, blue-shifted surface plasmon resonance (SPR) band at 302 nm, with the peak region spanning from 261 to 346 nm (Figure 33(d)). Unlike the typical SPR band for iron particles, which appears between 420 and 440 nm, the broad peak at 302 nm suggested the formation of small-sized magnetic photo-particles. Also, the peak intensity gradually decreased without a shoulder peak around 400 nm, likely due to the formation of iron oxide photo-particles as a result of the oxidation of zero-valent iron. The bandgap was subsequently calculated using

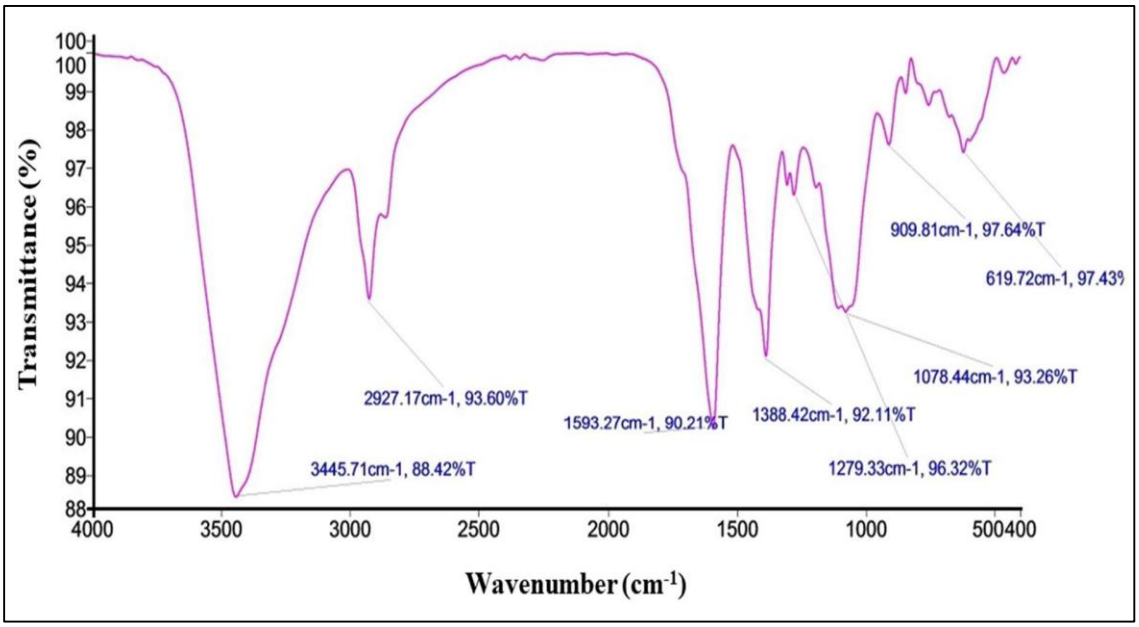
the Kubelka-Munk equation, and the results are graphically presented in Figure 32(d), indicating a bandgap of 3.01 eV. This suggests a strong electronic coupling between the materials, evidenced by the blueshift in the visible region (as shown in the inset). Therefore, CIMPI is capable of enhanced photodegradation reactions under visible light.



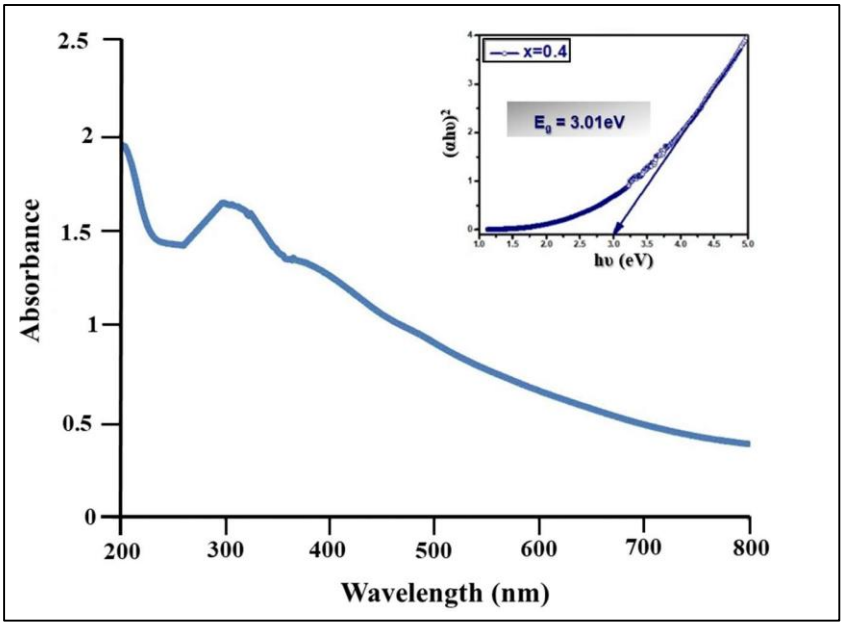
(a)



(b)



(c)



(d)

Fig.33 (a)X-ray diffraction pattern; (b) TGA; (c) FTIR; (d) UV-vis spectrum& Tauc Plot (band gap) of CIMPI

VII. BET Analyses

The specific surface area of the prepared optimal CIMPI was analyzed using Brunauer−Emmett−Teller (BET) analysis to assess its surface area. The N_2 adsorption-desorption isotherms of CIMPI in Figure 34, suggest a combination of type-II and type-IV isotherms, according to the IUPAC classification. The type-II portion implies unrestricted monolayer-multilayer adsorption, while the type-IV segment indicates hysteresis loop formation, typically associated with capillary condensation occurring in mesopores. This hysteresis loop signifies a limiting uptake observed over a range of high relative pressures.[23]The surface area of CIMPI found to be around 47.46 m^2/g, which is due to the presence of cellulase enzyme over magnetic iron. Pore diameter of CIMPI is found to be around 4.85 nm, which is mesoporous according to IUPAC definition.[24]

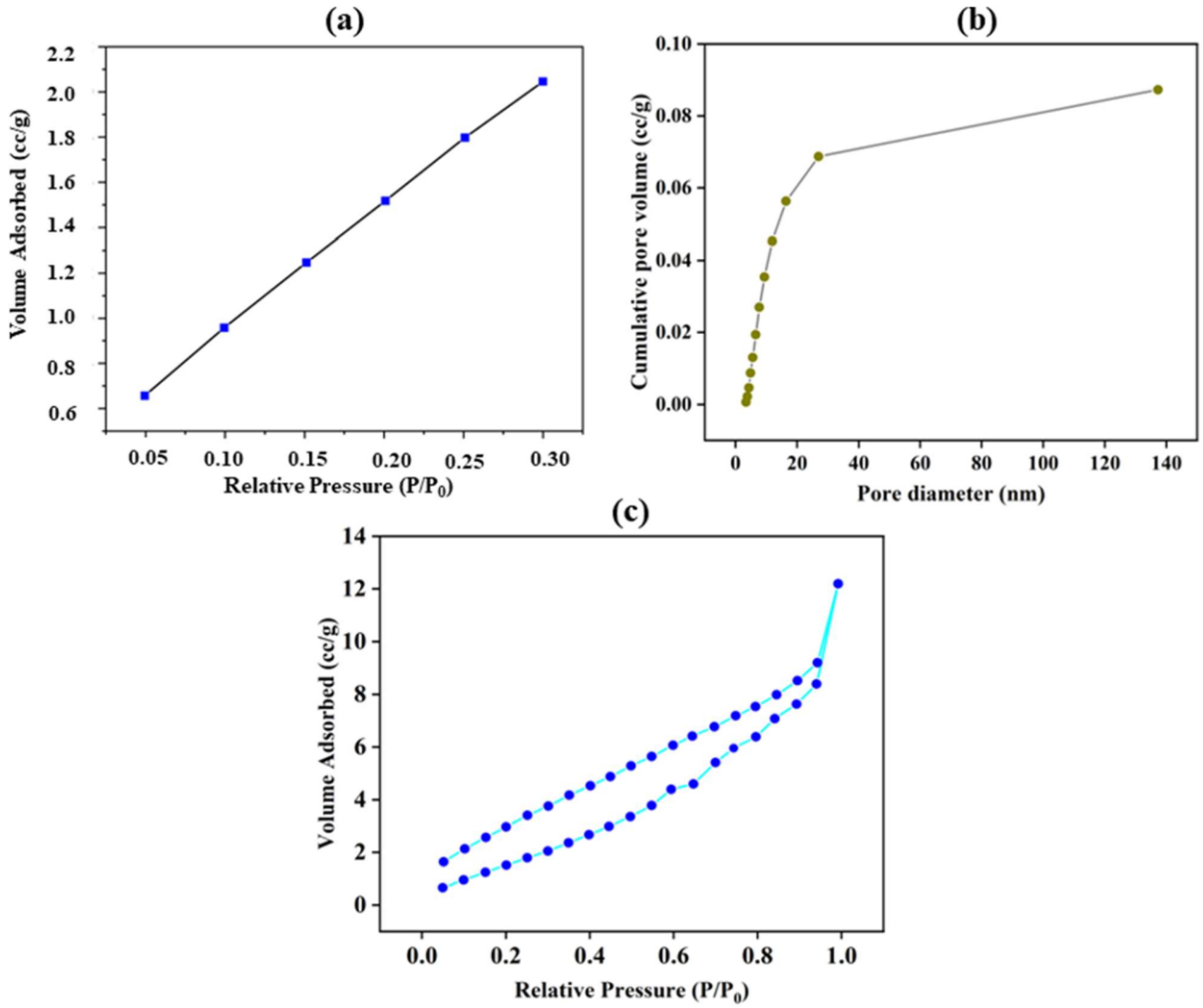


Fig. 34 a) Surface area isotherm**,** b) BJH plot and c) Adsorption isotherm depicting BET of CIMPI

VIII. Photoluminescence (PL) Spectroscopy

The fluorescence spectrum is widely utilized for assessing various processes such as carrier capture, migration, conversion, and separation, providing valuable insights into the separation of photo-generated electron-hole pairs.[25] The fluorescence spectrum predominantly consists of emission signals resulting from the recombination of photo-generated electron-hole pairs. A decrease in fluorescence intensity typically indicates higher separation efficiency of the charge carriers.[26] Figure 35 shows the photoluminescence spectra of CIMPI in a wavelength range of 545–745 nm. The intensity of CIMPI is 50000 which is similar to Fe_3O_4 particles, which shows the photo activity property is similar to the iron oxide particles. So, after synthesis of the CIMPI photo activity of the Fe_3O_4 particles present in the immobilized enzyme does not get affected.

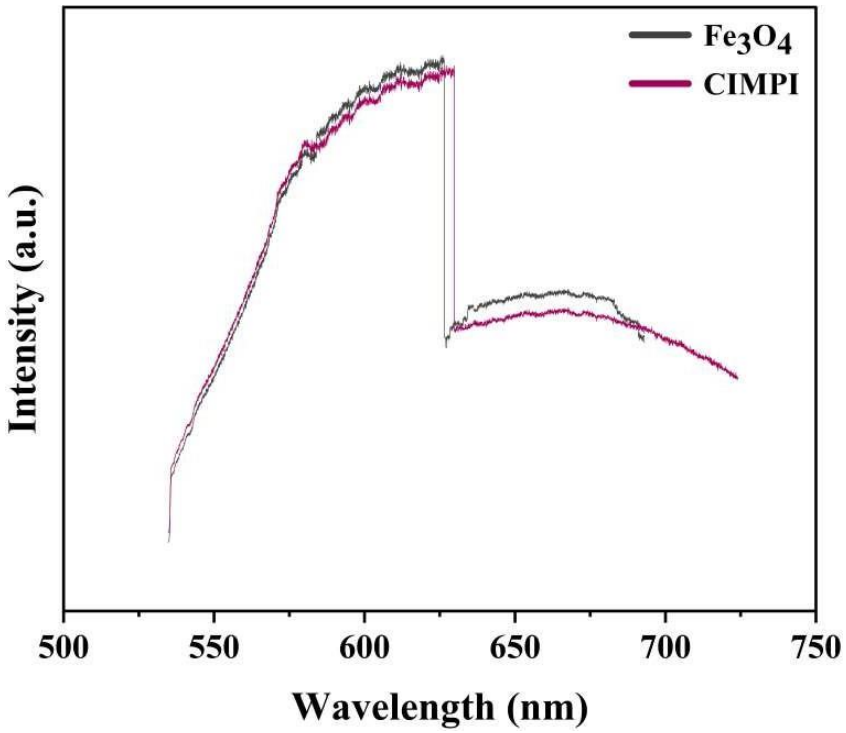


Fig.35 PL spectra of CIMPI

7.1.7 CIMPI Reusability Analysis

The residual activity relative to the initial activity was calculated for each cycle, and the impact of the cyclic index on cellulase activity is illustrated in Figure 36. It was observed that

as the number of cycles increased, the activity of immobilized cellulase gradually decreased. This decline was attributed to the repeated utilization of CIMPI, leading to the separation of cellulase from the immobilization carrier. Notably, till 6 cycles, the photoactive chemo-biocatalytic performance could still maintain upto 71% of the initial activity. However, after six cycles, the remaining activity of the CIMPI dropped to approximately 56%. This rapid decrease in activity was likely due to inactivation and leakage of the immobilized cellulase. Furthermore, the magnetic intensities of the immobilized carrier remained unaffected by the number of reuses. These findings indicate that the CIMPI could be efficiently utilized multiple times in the saccharification reaction.

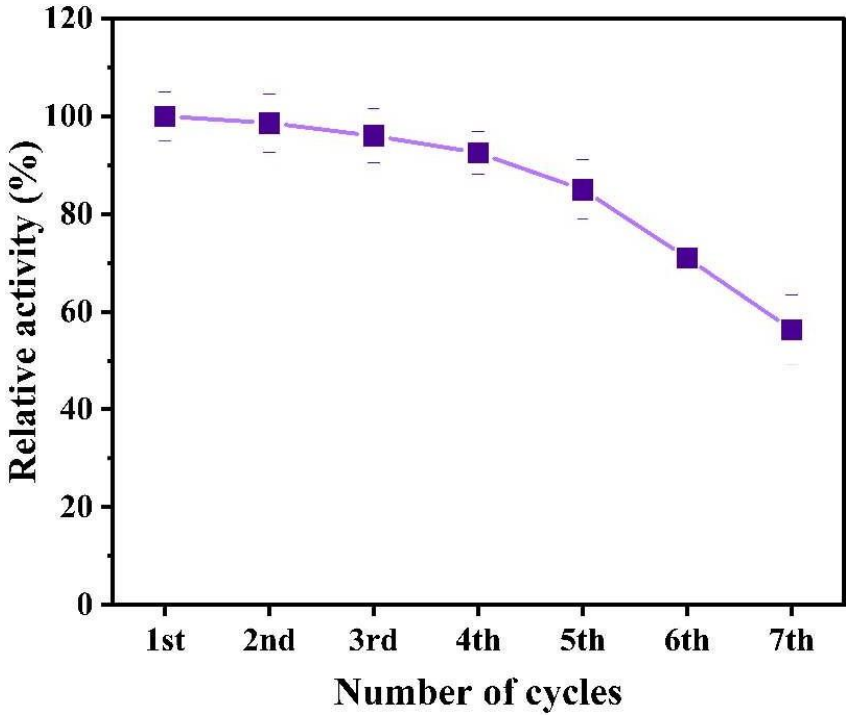


Fig. 36 CIMPI reusability cycles

7.1.8 CIMPI chemo-biocatalyst mechanism

Figure 37 illustrates the schematic of the proposed photo-chemo-bio mechanism of CIMPI. The cellulase enzyme breaks down insoluble cellulose into FS through the combined action of multiple enzymes, including endoglucanases, exoglucanases, and β-glucosidases.[27]Initially, the cellulase enzyme in the prepared CIMPI chemo-biocatalyst targets the β-1,4-glycosidic bonds in the cellulose chain, revealing the reducing and non-reducing ends of the cellulose chain by attacking the low-crystalline regions of the cellulose fiber with its endoglucanase activity. Subsequently, exoglucanase or cellobiohydrolase

activity targets the reducing and non-reducing ends of the cellulose chain, releasing monomers, eliminating sugar chains, and splitting cellobiose. Finally, β-glucosidase binds to cello-oligomers, hydrolyzing the β-1,4-glycosidic bonds of the cellulose polymer to break down cellulose and release FS from cellobiose. On the other hand, the Fe_3O_4 photoactive particles become excited under carbon infrared irradiation. This process allows the valence band (VB) electrons to surpass the energy barrier (Eg = 3.01 eV) and readily transfer to the conduction band (CB). The photons emitted by carbon infrared irradiation are absorbed by Fe_3O_4, initiating its photocatalytic activity. Consequently, this enhances the saccharification of PWBP, leading to an accelerated degradation reaction and an increased yield of FS which further on fermentation produced bio-ethanol.

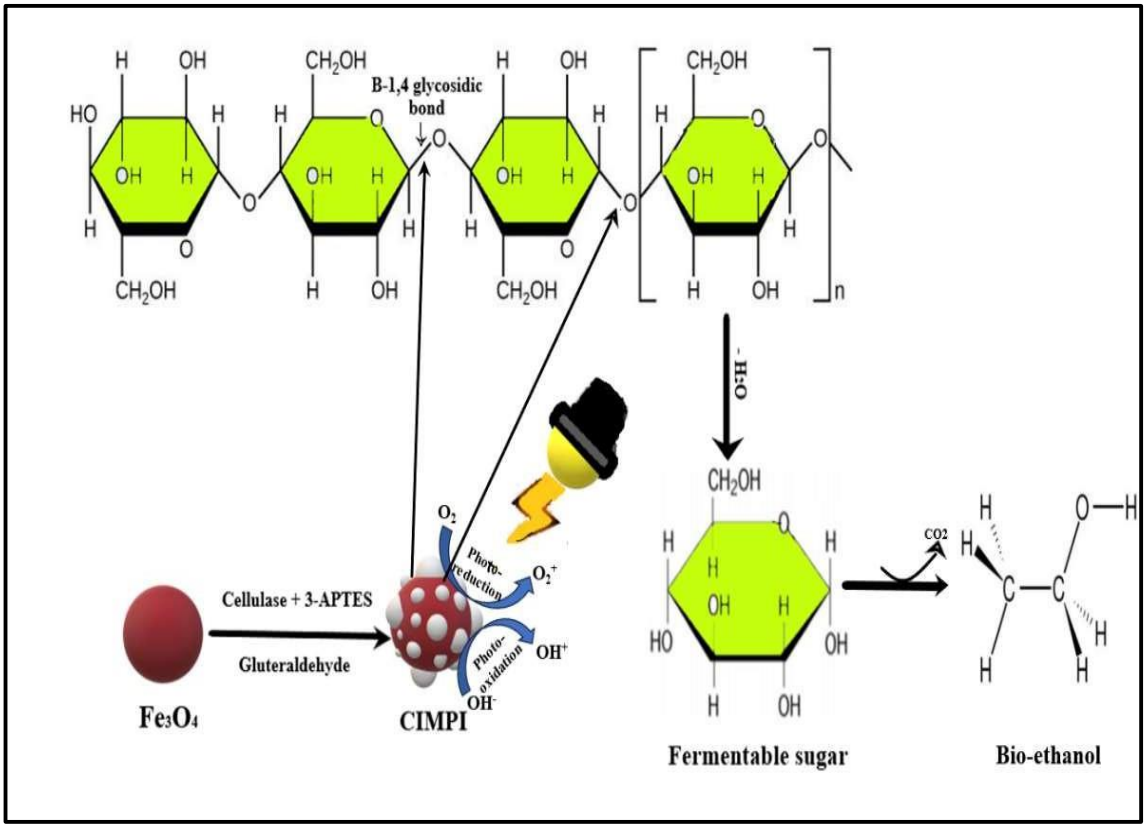


Fig.37 Plausible reaction mechanism of CIMPI chemo-biocatalyst

7.1.9 Energy efficiency of CIIVBR

One of the primary aims of this study was to evaluate the enhancement effects of CIIVBR on the saccharification process to achieve optimal conversion of PWBP to FS.[14]Under the

Taguchi-derived optimal conditions, it was observed that a peak yield of 73.4% $\ominus_{FS}$ was attained within a saccharification period of 60 min.Additionally, a maximum yield of 45.67% of $\ominus_{FS}$ was achieved using the free cellulase enzyme as the biocatalyst in the same duration. Conversely, in the conventional batch reactor (CBR), a gradual rise in glucose concentration over time was noted, indicative of a slower saccharification rate, resulting in a maximum yield of 58.22% $\ominus_{FS}$ using CIMPI, and a maximum yield of 36.54% of $\ominus_{FS}$ using free cellulase enzyme within the same 60min saccharification duration. Figure 38 effectively illustrates the variation in FS yield over time under optimal saccharification conditions using CIIVBR and CBR.

In this study, it is evident that CIIVBR (100W) significantly expedited the hydrolysis conversion process, thereby reducing both pretreatment and hydrolysis times required to achieve maximum FS yield compared to CSBR (500W). The utilization of CIIVBR led to a substantial amplification and intensification of PWBP to FS conversion due to the visible range irradiations generated by the carbon filament. These irradiations have the capability to penetrate the saccharification reaction mix deeply into various molecular layers, facilitating the efficient breakdown of BP crystalline structures through enhanced stretching and bending vibrations.[28] As a result, this promotes increased and faster depolymerization of cellulose/hemicellulose in the presence of the chemo-biocatalyst, leading to more severe molecular collisions. Conversely, CBR lacked these features, resulting in significantly lower conversion of PWBP to FS compared to CIIVBR. Additionally, it was observed that to achieve a maximum FS yield of 73.40 %, CIIVBR consumed 360kJ of energy, whereas CBR consumed 1800kJ of energy. Consequently, the energy consumption was 80% higher in CBR compared to CIIVBR, highlighting the superior energy efficiency of the novel CIIVBR.

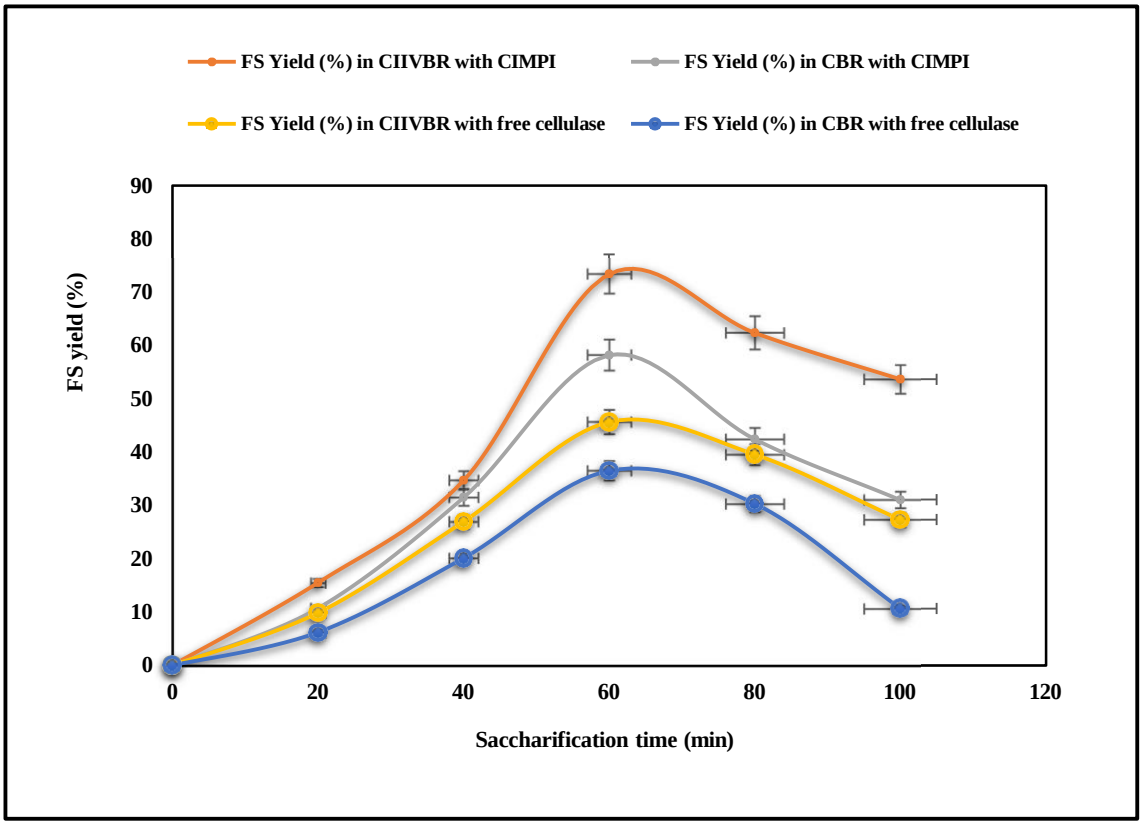


Fig.38 Variation in FS concentration with time during saccharification of PWBP employing CIIVBR and CBR using CIMPI and free cellulase enzyme

7.1.10 Analysis of bio-ethanol yield

Figure 39 shows bio-ethanol yield over time, where we can observe that after 12 h bio-ethanol yield increases up to 60 h exponentially and the bio-ethanol yield tends to get stationary after 60 h due to the depletion of fermentable sugar in the media. After 60 h 78.3% fermentable sugar can be converted into bio-ethanol. The highest bio-ethanol yield was obtained at 60 h around 24.2g/l.The fermentation efficiency was calculated to be 79.08 %. After purification 82.6 % concentrated bio-ethanol could be obtained. The alcohol by volume (ABV) % was determined to be 2.42% according to eqs 5.

Previous study on banana pseudostem and pineapple skin was separately carried out by Somaprabha[29] in 2022 using *Saccharomyces cerevisiae* for 72 h at 30° C which resulted in maximum bio-ethanol yield of 1.11g/g. Another study by Sukmaningtyas[30] in 2018 has shown applying SSF (simultaneous saccharification and fermentation) method using cellulase

enzyme and *Saccharomyces cerevisiae*for 120 h resulted in 4.32 g/L maximum bio-ethanol content. A study by Prakash et al.[31] in 2018 on banana peel fermentation resulted in 76.5% fermentation efficiency. This study reports higher fermentation efficiency in comparatively much lesser duration.

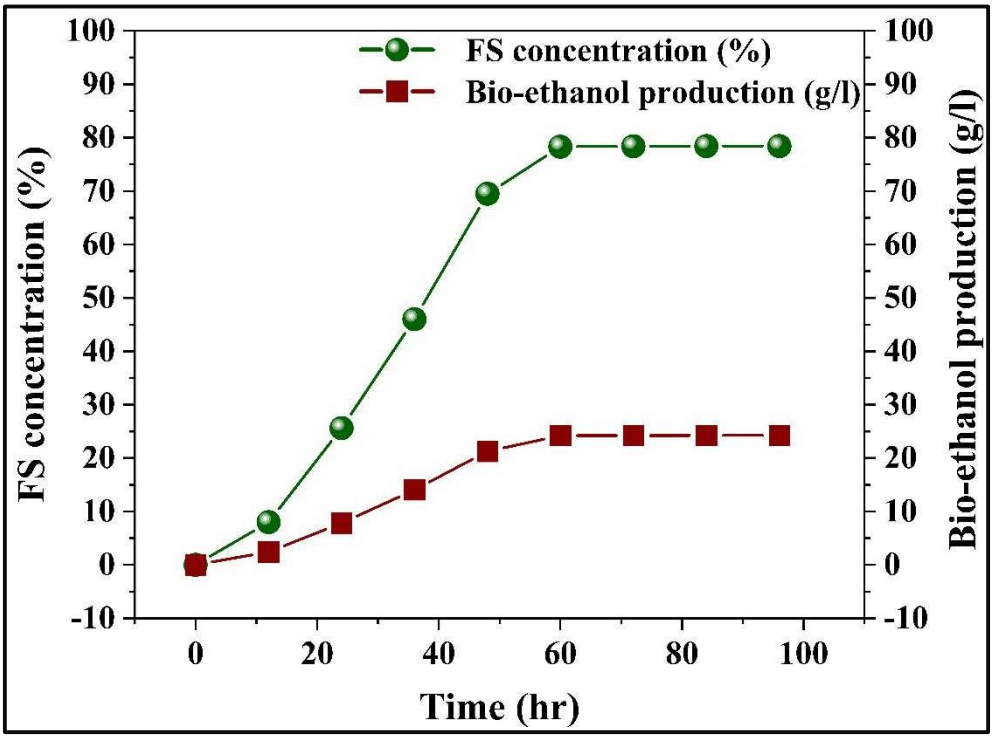


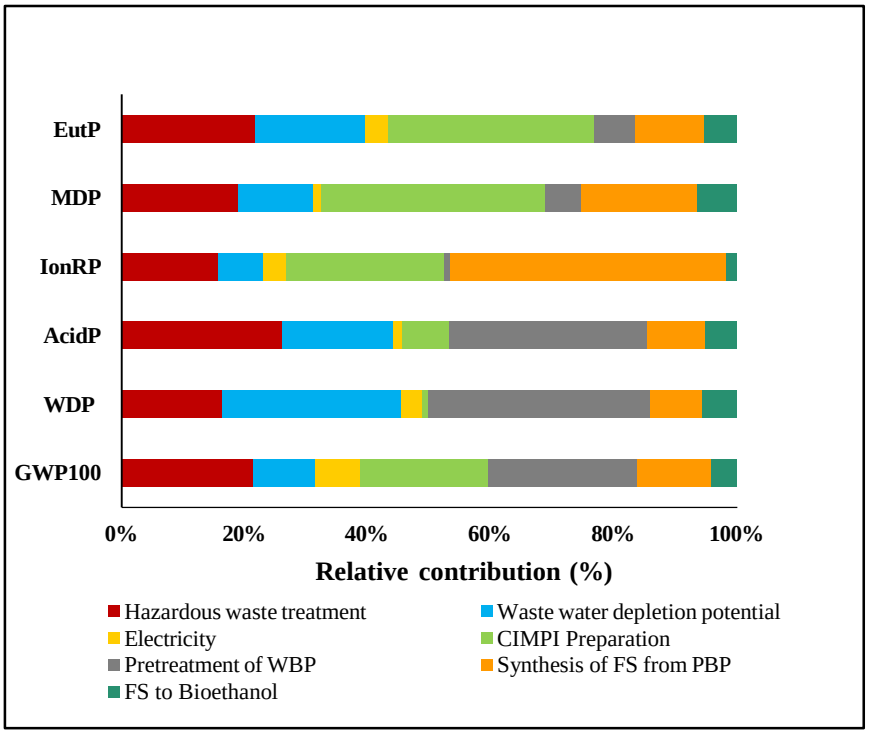
Fig.39 Bio-ethanol production (g/l) and fermentable sugar conversion (%) in every 12h

7.1.11 LCA analysis

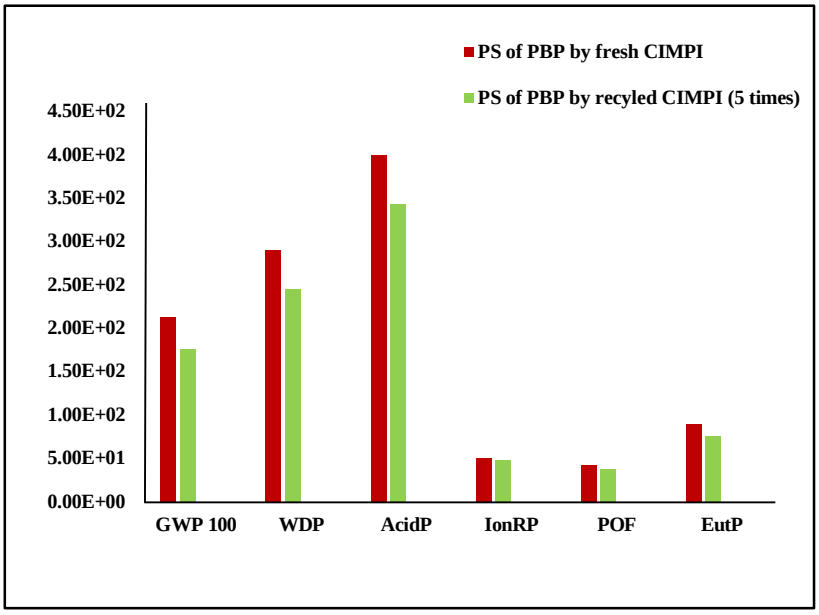
The outcomes of the environmental impact assessment, using ReCiPe Midpoint (H) v1.11, are illustrated in Figure 39 (a), (b), and (c) respectively. The findings identified the primary midpoint impact indicators for the two boundary system borders, which include Global Warming Potential (GWP100), Water Depletion Potential (WDP), Acidification Potential (AcidP), Ionizing Radiation Potential (IonRP), Metal Depletion Potential (MDP), and Eutrophication Potential (EutP).

Figure 40(a) shows that the pretreatment process of waste banana pseudostem has the highest environmental impact on GWP100, WDP, and AcidP indicators due to the substantial use of acetic acid. Meanwhile, CIMPI preparation is the main contributor to MDP and EutP. The primary reason for its significant impact on these indicators is the use of metal precursors in

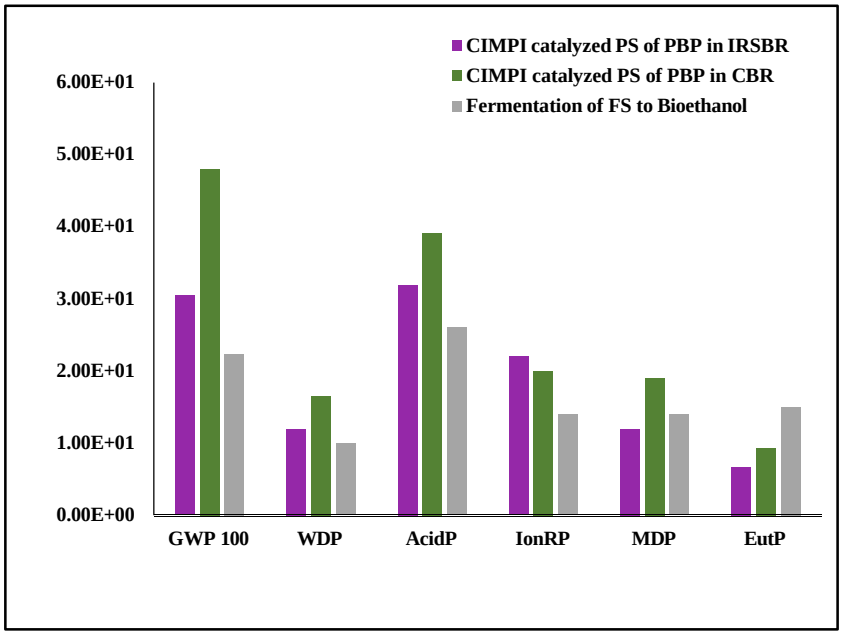
the photo-biocatalyst preparation process. Additionally, the synthesis of FS from pretreated banana pseudostem (PWBP) had the highest IonP due to the use of infrared radiation in the reaction. In contrast, the production of bio-ethanol from FS significantly lowered the GWP indicator and other environmental impacts. Furthermore, the photo-biocatalytic-saccharification method with 6 cycles of recycled CIMPI had a lesser environmental impact compared to using fresh CIMPI, as depicted in Figure 40(b).The CIMPI-catalyzed photo-biocatalytic saccharification (PS) of PWBP in the CIIVBR showed reduced impacts in all categories compared to PS in the CBR, as depicted in Figure 40(c). This underscores the efficiency of the CIIVBR heating system over the conventional system. Notably, the GWP100 was reduced by 37.5%, AcidP by 18.36%, and WDP by 27.27% with the novel reactor. Furthermore, the fermentation of FS to bio-ethanol significantly reduces all impact factors even more compared to the PS of PWBP in the CIIVBR.



(a)



(b)



(c)

Fig.40 (a) Relative percentage contribution of different sub processes covering the boundary system;(b) Comparative environmental impact analysis of recycled CIMPI over fresh CIMPI; (c) Comparative environmental impacts of CIIVBR, CBR, and FS to bio-ethanol

7.2 Results and discussion for PL to FS conversion using CIPSn

7.2.1 PL and PPL composition analysis

To determine the sample's holo-cellulose and lignin content, the chemical composition of PL and PPL were measured. According to the preliminary analysis, the weight percentage composition of the PL in this study is 76 wt.% cellulose, 17 wt.% hemicellulose, 5 wt.% lignin, and 2 wt.% others. The physical pretreatment of PL made it expedient for the chemical pretreatment with peracetic acid. After treatment with peracetic acid under carbon irradiation in CIIVBR 78 wt.% of isolated lignin (purity 97%) could be attained.

7.2.2 FS yield analysis via UV Spectroscopy

By analyzing the standard curve graph, the correlation between UV absorbance at 540nm and glucose concentration in mg/ml was determined. Subsequently, employing the eqs 3, the yield of FS was calculated to be 56.20%.

7.2.3 Optimization of FS yield

Table 11. Representing 9 experimental runs as per L9TED using CIPSn

Temperature (°C)	Time (min)	PL: CIPSn	Yield %	SNRA1
40	45	10:1	25.62	28.1716
40	65	10:2	28.33	29.0449
40	85	10:3	29.21	29.3106
60	45	10:2	30.33	29.6374
60	65	10:3	31.10	29.8552
60	85	10:1	32.50	30.2377
80	45	10:3	36.72	31.2981
80	65	10:1	40.30	32.1061
80	85	10:2	56.20	34.9947

Taking 9 runs designed from Taguchi optimization method, maximum sugar yield of 56.20 % can be achieved in the subsequent hydrolysis process at 85 min, 80 °C temperature with 10:2 biomass and CIPSn ratio.

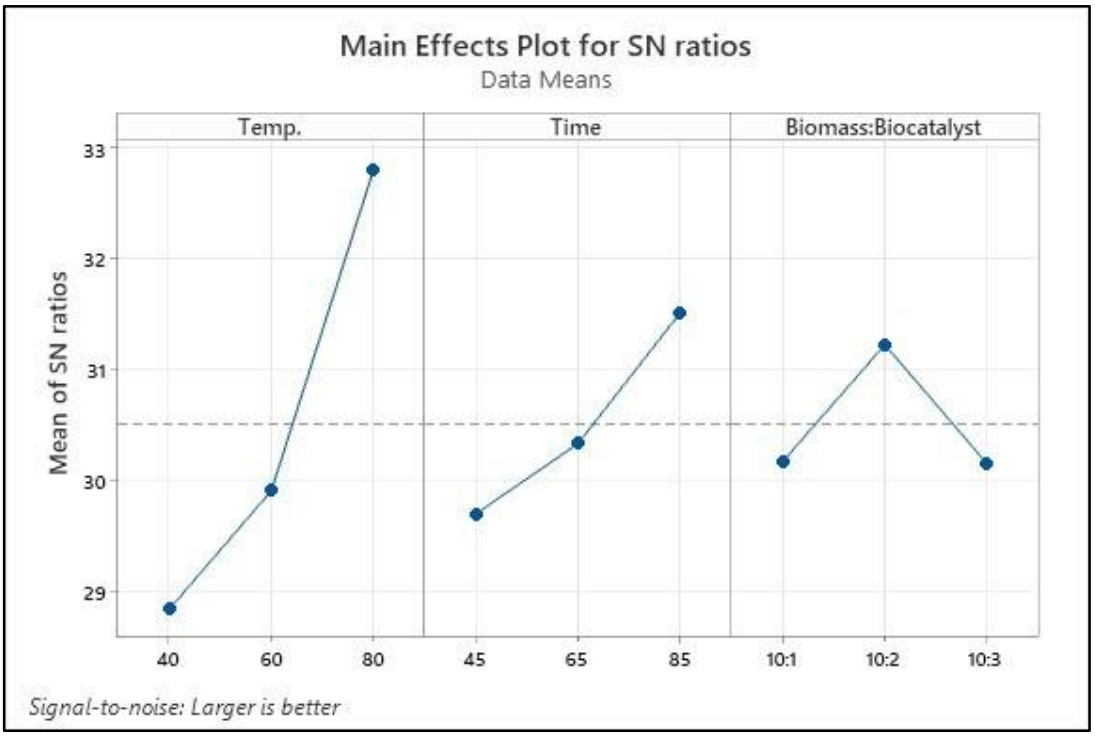


Fig.41 Main effects plot for SN ratio

7.2.4 Characterization of the prepared optimal chemo-biocatalyst

I. XRD Analysis

XRD analysis of CIMPI was done to detect the crystal structure of cellulose and Sn by shining X-rays onto those samples and measuring the angles and intensities of the X-rays that are scattered by the sample's atomic planes. The analysis was done at 2Θ angle ranging from 20°to 75° with a scanning speed of 1° per minute using a Cu Kα source and an Intel CPS 120 hemispherical detector manufactured by Rigaku Miniflex Co. in Japan. In Figure 42 at 2Θ = 26.6°, 33.9°, 38.1°, 51.9° crystalline peak of tin oxide can be seen and at 2Θ = 24.32°, 27.65°, 40.33°, 45.28°, 55.12°, 58.92° crystalline peak of Si can be seen due to the presence of Si in APTES.

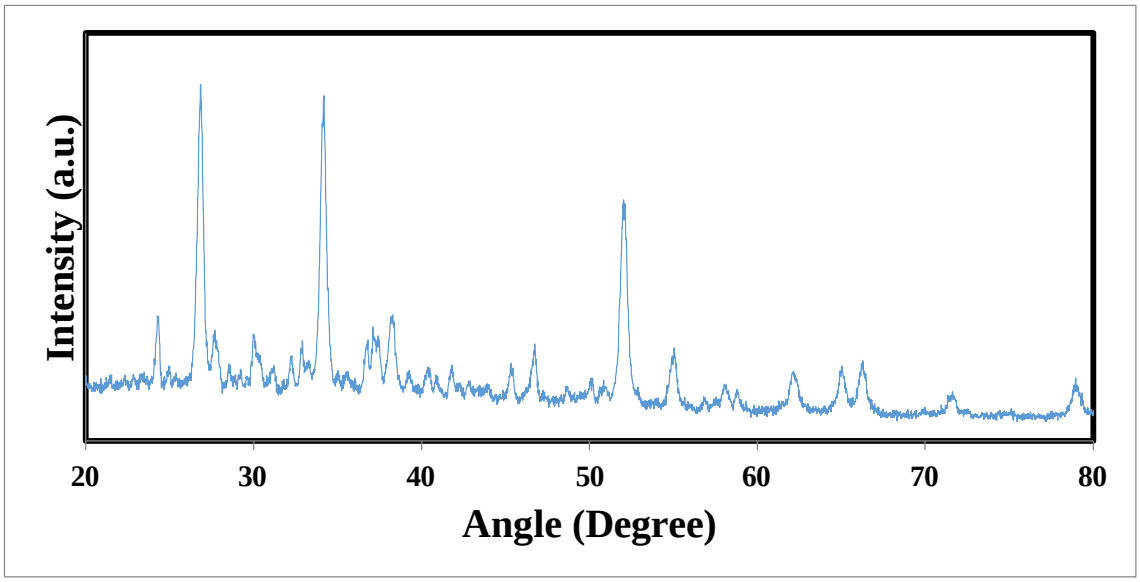


Fig.42 XRD pattern of CIPSn

II. FTIR Analysis

FTIR analysis of CIPSn (Figure 43) reveals crucial insights into its molecular structure and surface properties. The spectrum typically exhibits characteristic peaks representing various functional groups and bonding within the material. The broad peak in the range of 3200-3600 cm^{-1} signifies the O-H stretching vibration, indicative of hydroxyl groups associated with surface hydroxyls or absorbed water molecules. Another prominent feature is the peak around 500-800 cm^{-1} attributed to Metal-O stretching vibrations, reflecting the bonds between tin and oxygen atoms in the SnO_2 lattice. Additionally, deviations or shifts in this region may suggest the presence of oxygen vacancies, highlighting defects or deviations from the stoichiometric composition. Peaks within the 1500-1700 cm^{-1} range correspond to bending vibrations of surface hydroxyl groups (OH), emphasizing interactions occurring on the SnO_2 surface. Moreover, peaks within the 1000-1500 cm^{-1} region may signal the presence of adsorbed species like carbonates, water, or organic contaminants, proving the presence of SnO_2 in the prepared CIPSn chemo-bio catalyst.

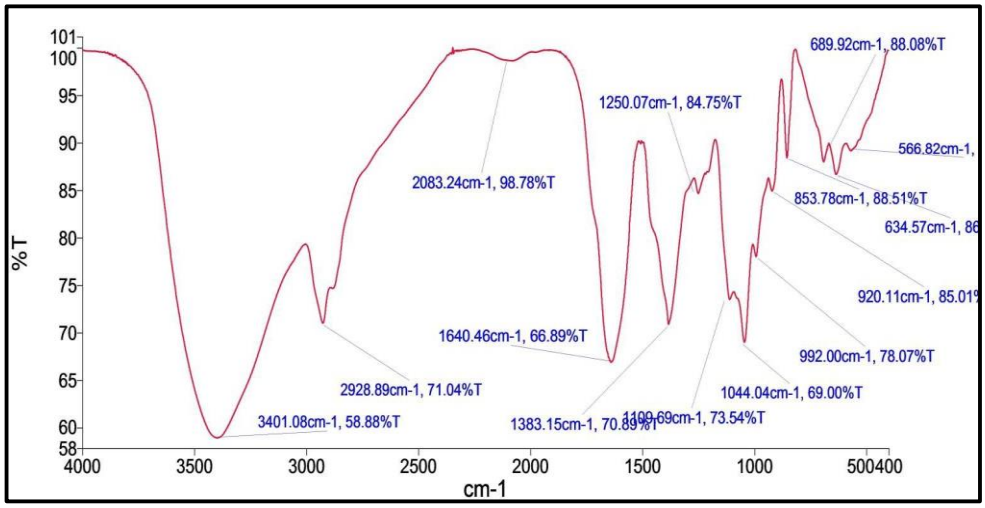


Fig.43 FTIR of CIPSn

III. TGA Analysis

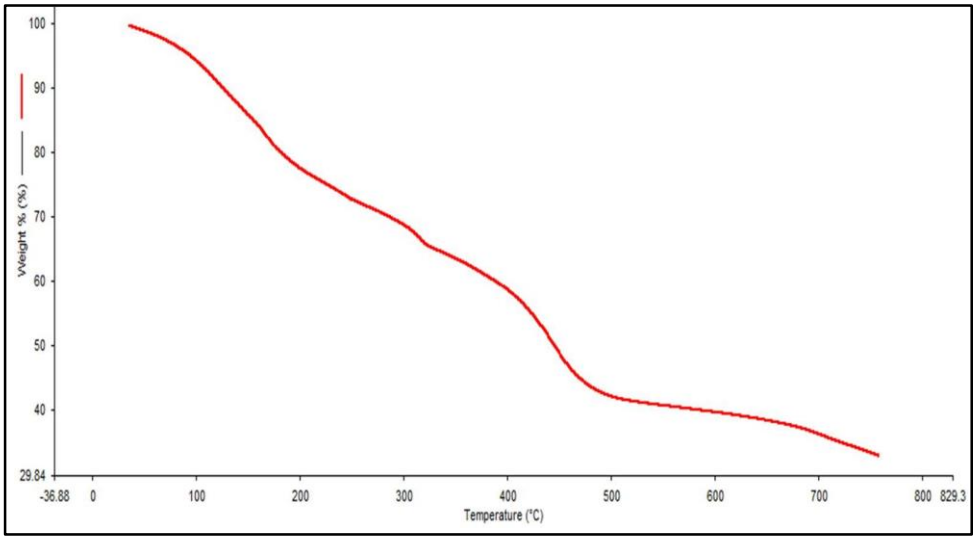


Fig. 44 TGA Plot of CIPSn

In Figure 44 a weight loss of around 10% can be seen before 150 °C which is due to the release of unbound moisture from CIPSn. From temperature 150-320 °C a significant weight loss of 10% can be observed due to the release of unbound moisture from the CIPSn sample. After 320 °C temperature there is a steady fall can be observed in the TGA plot till 500 °C which is due to the combustion of cellulase and other organic substances.

CHAPTER 8

CONCLUSION

&

FUTURE SCOPE

8.1 Conclusion

The study successfully demonstrates the development and application of a sustainable cellulase immobilized magnetic-photoactive iron (CIMPI) chemo-biocatalyst for the efficient valorization of waste banana pseudostem (WBP) into fermentable sugars (FS) using an innovative carbon-infrared irradiated vibrating batch reactor (CIIVBR). By optimizing the pretreatment and saccharification processes, the study achieved a high FS yield of 73.40%, underscoring the effectiveness of the CIMPI in conjunction with the energy-efficient CIIVBR system. The optimal CIMPI exhibited excellent photoactive properties, with a bandgap of 3.01 eV, and demonstrated efficient recovery and recyclability due to its magnetic properties. Moreover, the CIIVBR showed remarkable energy savings of up to 80% compared to conventional batch reactors (CBR) under optimal conditions, highlighting its superior energy efficiency. Subsequent conversion of the optimally produced FS into bio-ethanol using dry yeast (*Saccharomyces cerevisiae*) resulted in maximum24.2 g/l bio-ethanol yield in 60 h with 79.08 %efficiency. The life cycle assessment (LCA) revealed significant environmental benefits, including a reduction in Global Warming Potential (GWP100) by 37.5 %, Acidification Potential (AcidP) by 18.36 %, and Water Depletion Potential (WDP) by 27.27 % compared to conventional processes.

In conclusion, this study not only demonstrates an efficient process to waste banana pseudostem valorization but also emphasizes on the advantages of the CIIVBR-CIMPI system with substantial environmental sustainability. The developed technology showcases potential for contributing to the development of green and sustainable biofuel production from similar lignocellulosic biomasses while significantly mitigating environmental impacts.

8.2 Future scope of work

Phase 1: Process Modification and Integration

✓ To conduct an extensive literature review to gather information on lignocellulosic biomass characteristics, its suitability as feedstock, and existing conversion processes.

✓ To synthesize similar catalysts using other photoactive magnetic metals.

✓ To improve bioethanol yield by using better fermentation condition and genetically modified micro-organisms and evaluation of any other products if produced.

✓ To create comprehensive model of the modified process using Aspen Plus software.

✓ To validate the model by comparing simulation results with available experimental data from the existing batch process.

Phase 2: Scale-up Analysis

✓ To conduct a feasibility study to assess the economic and technical viability of scaling up the process.

✓ To investigate the potential challenges and constraints in scaling up, and propose mitigation strategies.

Phase 3: Cost Analysis

✓ To costs analyze and determine the economical sustainability of the prosess.

CHAPTER 9

REFERENCES

References

Khoshnevisan, K., Vakhshiteh, F., Barkhi, M., Baharifar, H., Poor-Akbar, E., Zari, N., ... &Bordbar, A. K. (2017). Immobilization of cellulase enzyme onto magnetic particles: Applications and recent advances. Molecular Catalysis, 442, 66-73.

Zang, L., Qiu, J., Wu, X., Zhang, W., Sakai, E., & Wei, Y. (2014). Preparation of magnetic chitosan particles as support for cellulase immobilization. Industrial & engineering chemistry research, 53(9), 3448-3454.

Khoshnevisan, K., Bordbar, A. K., Zare, D., Davoodi, D., Noruzi, M., Barkhi, M., &Tabatabaei, M. (2011). Immobilization of cellulase enzyme on superparamagnetic particles and determination of its activity and stability. Chemical engineering journal, 171(2), 669-673.

Lima, J. S., Araújo, P. H., Sayer, C., Souza, A. A., Viegas, A. C., & de Oliveira, D. (2017). Cellulase immobilization on magnetic particles encapsulated in polymer spheres. Bioprocess and biosystems engineering, 40, 511-518.

Ladole, M. R., Mevada, J. S., &Pandit, A. B. (2017). Ultrasonic hyperactivation of cellulase immobilized on magnetic particles. Bioresource technology, 239, 117-126.

Selvam, K., Govarthanan, M., Senbagam, D., Kamala-Kannan, S., Senthilkumar, B., &Selvankumar, T. (2016). Activity and stability of bacterial cellulase immobilized on magnetic particles. Chinese Journal of Catalysis, 37(11), 1891-1898.

Mubarak, N. M., Wong, J. R., Tan, K. W., Sahu, J. N., Abdullah, E. C., Jayakumar, N. S., &Ganesan, P. (2014). Immobilization of cellulase enzyme on functionalized multiwall carbon tubes. Journal of Molecular Catalysis B: Enzymatic, 107, 124-131.

Han, J., Luo, P., Wang, Y., Wang, L., Li, C., Zhang, W., ... & Ni, L. (2018). The development of biocatalysis via the immobilization of cellulase on composite magnetic material for enhanced loading capacity and catalytic activity. International journal of biological macromolecules, 119, 692-700.

Bindra S, Sharma R, Khan A, Kulshrestha S. Renewable energy sources in different generations of bio-fuels with special emphasis on microalgae derived biodiesel as sustainable industrial fuel model. Biosciences Biotechnology Research Asia. 2017 Mar 25;14(1):259-74.

MH Hassan, MAKalam. An overview of biofuel as a renewable energy source: development and challenges. Procedia Engineering. 2013 Jan 1; 56:39-53.

Kour D, Rana KL, Yadav N, Yadav AN, Rastegari AA, Singh C, Negi P, Singh K, Saxena AK. Technologies for biofuel production: current development, challenges, and future prospects. Prospects of renewable bioprocessing in future energy systems. 2019:1-50.

Searchinger TD. Biofuels and the need for additional carbon. Environmental Research Letters. 2010 Jun 1;5(2):024007.

Bessou C, Ferchaud F, Gabrielle B, Mary B. Biofuels, greenhouse gases and climate change. Sustainable Agriculture Volume 2. 2011:365-468.

Meidan M. The outlook for China' s fossil fuel consumption under the energy transition and its geopolitical implications. OIES Paper: CE; 2023.

Olaganathan, R., Ko Qui Shen, F., & Jun Shen, L. (2014). Potential and technological advancement of biofuels. International Journal of Advanced Scientific and Technical Research,4(4), 12.

Ibeto, C. N., Ofoefule, A. U., & Agbo, K. E. (2011). A global overview of biomass potentials for bioethanol production: a renewable alternative fuel. Trends in Applied Sciences Research, 6(5),410.

Peskett, L., Slater, R., Stevens, C., & Dufey, A. (2007). Biofuels, agriculture and poverty reduction. Natural resource perspectives, 107, 1-6.

Van der Horst, D., & Vermeylen, S. (2011). Spatial scale and social impacts of biofuel production. Biomass and bioenergy, 35(6), 2435-2443.

Teferra, B. T. (2022). Designing and planning of Ethiopia's biomass-to-biofuel (bioethanol and biodiesel) supply chain through integrated strategic-tactical optimization model under economic and environmental dimensions.

Gatdula, K. M., Blaquera, M. S. F. N., Jimena, C. M. V., Elegado, F. B., Alcantara, J. Z., & Guerrero, G. A. M. (2021, May). A comparative study on bioethanol production from rice straw and banana pseudostem through simultaneous saccharification and fermentation using Kluyveromycesmarxianus. In IOP Conference Series: Earth and Environmental Science (Vol. 765, No. 1, p. 012006). IOP Publishing.

Sukmaningtyas, R. P. (2018). Pretreated of banana pseudo-stem as raw material for enzymatic hydrolysis and bioethanol production. In MATEC Web of Conferences (Vol. 154, p. 01035). EDP Sciences.

Ingale, S., Joshi, S. J., &Gupte, A. (2014). Production of bioethanol using agricultural waste: banana pseudo stem. Brazilian Journal of Microbiology, 45, 885-892.

Souza, E. L., Lieblb, G. F., Marangonia, C., Sellina, N., Montagnolia, M. S., & Souza, O. (2014). Bioethanol from fresh and dried banana plant pseudostem. Chemical engineering transactions, 38.

Ferreira da Silva, I., Reis FontinelleSouto, L., Collins, S. R., Elliston, A., de Queiroz, J. H., & Waldron, K. W. (2020). Impact of hot water and alkaline pre-treatments in cellulosic ethanol production from banana pseudostem. BioEnergy Research, 13, 1159-1170.

VN, P., S Krishna, S., J Kings, A., & LR, M. M. (2018, April). Potential Bioethanol Production from Agricultural Banana Waste. In International Conference on Energy Efficient Technologies for Sustainability (ICEETS).

Araguirang, G. E., Arizala, A. J. R., Asilo, E. B. B., Batalon, J. L. S., Bello, E. B., Madigal, J. P. T., ... &Elegado, F. B. (2020). Pre-treatment And Enzymatic Hydrolysis Of Banana (Musa Acuminata X Balbisiana) Pseudostem For Ethanol Production. Agro Bali: Agricultural Journal, 3(2), 98-107.

Legodi, L. M., LaGrange, D. C., Jansen van Rensburg, E. L., &Ncube, I. (2021). Enzymatic hydrolysis and fermentation of banana pseudostem hydrolysate to produce bioethanol. International Journal of Microbiology, 2021, 1-14.

Consumption volume of ethanol as fuel in India 2013-2023. Published by Madhumitha Jaganmohan, Jan 2, 2024

Dilkushi, H. A. S., Jayarathna, S., Manipura, A., Chamara, H. K. B. S., Edirisinghe, D., Vidanarachchi, J. K., & Priyashantha, H. (2024). Development and characterization of biocomposite films using banana pseudostem, cassava starch and poly (vinyl alcohol): A sustainable packaging alternative. Carbohydrate Polymer Technologies and Applications, 7, 100472.

Laltha, M., Sewsynker-Sukai, Y., & Gueguim Kana, E. B. (2024). Innovative microwave-assisted iodized table salt or paper wastewater pretreatments for enhanced sugar recovery from banana pseudostem. Biomass Conversion and Biorefinery, 14(3), 4139-4153.

Samara, F. S., Novia, N., & Melwita, E. (2024). Enzymatic hydrolysis of cellulose banana stem (alkaline microwave-assisted pre-treatment). Journal of Integrated and Advanced Engineering (JIAE), 4(1), 21-30.

Shaji, A., Alex, S., George, A. M., Nair, D. S., Aparna, B., & Soni, K. B. (2024). Enhancement of bioethanol production from lignocellulosic biomass of banana by single batch fermentation using Saccharomyces cerevisiae and native microorganism. Environment Conservation Journal.

Wang, T., Nolte, M. W., & Shanks, B. H. (2014). Catalytic dehydration of C 6 carbohydrates for the production of hydroxymethylfurfural (HMF) as a versatile platform chemical. Green Chemistry, 16(2), 548-572.

Luo, Z., Zheng, Z., Li, L., Cui, Y. T., & Zhao, C. (2017). Bimetallic Ru–Ni catalyzed aqueous-phase guaiacol hydrogenolysis at low H2 pressures. Acs Catalysis, 7(12), 8304-8313.

Huang, Y. B., & Fu, Y. (2013). Hydrolysis of cellulose to glucose by solid acid catalysts. Green chemistry, 15(5), 1095-1111.

Sabiha-Hanim, S., & Abd Halim, N. A. (2018). Sugarcane bagasse pretreatment methods for ethanol production. Fuel ethanol production from sugarcane, 63-79.

Sun, S. L., Chen, V. Z., Sunny, S. A., & Chen, J. (2019). Venture capital as an innovation ecosystem engineer in an emerging market. International Business Review, 28(5), 101485.

Ager, D. J., de Vries, A. H., & de Vries, J. G. (2012). Asymmetric homogeneous hydrogenations at scale. Chemical Society Reviews, 41(8), 3340-3380.

Shirkavand, E., Baroutian, S., Gapes, D. J., & Young, B. R. (2016). Combination of fungal and physicochemical processes for lignocellulosic biomass pretreatment–a review. Renewable and Sustainable Energy Reviews, 54, 217-234.

Barman, S., & Chakraborty, R. (2024). Energy-efficient and eco-friendly continuous production of 5-CMF in a UV-ultrasound irradiated catalytic packed bed reactor:

heterogeneous kinetics, reactor simulation and LCA analysis. Reaction Chemistry & Engineering, 9(1), 160-171.

Nwufo, O. C.; Nwafor, O. M. I.; Igbokwe, J. O. Effects of blends on the physical properties of bio-ethanol produced from selected Nigerian crops.Int. J. Ambient Energy. 2016, 37, 10-15.

Lynd, L. R.; Cushman, J. H.; Nichols, R. J.; Wyman, C. E. Fuel ethanol from cellulosic biomass. Science 1991, 251, 1318-1323.

Masum, B. M.; Masjuki, H. H.; Kalam, M. A.; Palash, S. M.; Wakil, M. A.; Imtenan, S. Tailoring the key fuel properties using different alcohols (C2–C6) and their evaluation in gasoline engine.Energy Convers. Manage. 2014, 88, 382-390.

VN, P.; S Krishna, S.; J Kings, A.; LR, M. M. (, April). Potential Bio-ethanol Production from Agricultural Banana Waste. ICEETS. 2018.

Balat, M. Production of bio-ethanol from lignocellulosic materials via the biochemical pathway: a review.Energy Convers. Manage. 2011, 52, 858-875.

Naik, S. N.; Goud, V. V.; Rout, P. K.; Dalai, A. K. Production of first and second generation biofuels: a comprehensive review. Renewable Sustainable Energy Rev. 2010, 14, 578-597.

Sharma, N.; Sharma, N. Second generation bio-ethanol production from lignocellulosic waste and its future perspectives: a review. Int J Curr Microbiol Appl Sci. 2018, 7, 1285-1290.

Callegari, A.; Bolognesi, S.; Cecconet, D.; Capodaglio, A. G. Production technologies, current role, and future prospects of biofuels feedstocks: A state-of-the-art review. Critical Reviews in Environmental Science and Technology. 2020, 50, 384-436.

Devi, A.; Bajar, S.; Sihag, P.; Sheikh, Z. U. D.; Singh, A.; Kaur, J.; Pant, D. A panoramic view of technological landscape for bio-ethanol production from various generations of feedstocks. Bioengineered. 2023, 14, 81-112.

Adsal, K. A.; ÜÇTUĞ, F. G.; Arikan, O. A. Environmental life cycle assessment of utilizing stem waste for banana production in greenhouses in Turkey.Sustainable Prod. Consumption. 2020, 22, 110-125.

Abeln, F., & Chuck, C. J. (2020). The role of temperature, pH and nutrition in process development of the unique oleaginous yeast Metschnikowia pulcherrima. Journal of Chemical Technology & Biotechnology, 95(4), 1163-1172.

Mohiuddin, A. K. M.; Saha, M. K.; Hossian, M. S.; Ferdoushi, A. Usefulness of banana (Musa paradisiaca) wastes in manufacturing of bio-products: a review. The Agriculturists. 2014, 12, 148-158.

Chen, S. C.; Duan, K. J. Production of galactooligosaccharides using β-galactosidase immobilized on chitosan-coated magnetic particles with tris (hydroxymethyl) phosphine as an optional coupling agent.Int. J. Mol. Sci. 2015,16, 12499-12512.

Khoshnevisan, K.; Bordbar, A. K.; Zare, D.; Davoodi, D.; Noruzi, M.; Barkhi, M.; Tabatabaei, M. Immobilization of cellulase enzyme on superparamagnetic particles and determination of its activity and stability.Chem. Eng. J. 2011, 171, 669-673.

Roy Choudhury, S.; Chakraborty, R. Intensified wheat husk conversion employing energy-efficient hybrid electromagnetic radiations for production of fermentable sugar: process optimization and life cycle assessment. Environ. Sci. Pollut. Res. 2021, 28, 58902-58914.

Abraham RE; Verma ML; Barrow CJ; Puri M. Suitability of magnetic nano particle immobilised cellulases in enhancing enzymatic saccharification of pretreated hemp biomass. Biotechnol Biofuels. 2014, 7, 90

Xu J; Huo S; Yuan Z; Zhang Y; Xu H; Guo Y; Liang C; Zhuang X. Characterization of direct cellulase immobilization with super paramagnetic nano particles. Biocatal Biotransform. 2011, 29, 71–76

Lu PJ; Fu WE; Huang SC; Lin CY; Ho ML; Chen YP; Cheng HF. Methodology for sample preparation and size measurement of commercial ZnO nano particles. J Food Drug Anal. 2018, 26, 628–636

Burgula Y; Khali D; Kim S; Krishnan SS; Cousin MA; Gore JP; Reuhs BL; Mauer LJ. Detection of Escherichia coli O157:H7 and Salmonella typhimurium using filtration followed by Fourier-transform infrared spectroscopy. J Food Prot. 2006, 69, 1777–1784

Miller, G. (1959). Determination of reducing sugar by DNS method. Anal. Chem, 31, 426-428.

Roy Choudhury, S.; Chakraborty, R. Sustainable Total Reducing Sugar Production by Waste Printed Power Board Derived Zn–Zr Photocatalyst. Waste Biomass Valorization. 2023, 14, 3603-3619.

Namchot W; Panyacharay N; Jonglertjunya W; Sakdaronnarong C. Hydrolysis of delignified sugarcane bagasse using hydrothermal technique catalyzed by carbonaceous acid catalysts. Fuel 2014, DOI: 10.1016/j.fuel.2013.08.062

Muley, A. B.; Mulchandani, K. H.; Singhal, R. S. Immobilization of enzymes on iron oxide magnetic nanoparticles: synthesis, characterization, kinetics and thermodynamics. Methods Enzymol. 2020, DOI: 1016/bs.mie.2019.10.016

Saini, D. S.; Tripathy, S.; Kumar, A.; Sharma, S. K.; Ghosh, A.; Bhattacharya, D. Impedance and modulus spectroscopic analysis of single phase BaZrO3 ceramics for SOFC application. Ionics. 2018, 24, 1161-1171.

Naik, B.; Ghosh, N. N. A review on chemical methodologies for preparation of mesoporous silica and alumina based materials. Recent patents on technology. 2009, 3, 213-224**.**

Yu, J. C.; Yu, J.; Ho, W.; Jiang; Zhang. Effects of F-doping on the photocatalytic activity and microstructures of crystalline TiO2 powders.Chem. Mater. 2002, 14, 3808-3816.

Cao, Y.; Li, C.; Li, J.; Li, Q.; Yang, J. Magnetically separable Fe 3 O 4/AgBr hybrid materials: highly efficient photocatalytic activity and good stability.Nanoscale Res. Lett. 2015, 10, 1-6.

Choudhury, S. R.; Das, A.; Chakraborty, R. Review on progress in cellulase catalyzed saccharification of agricultural lignocellulosic biomass towards fermentable sugar and bioethanol: Kinetics & reactor configurations. Biocatal. Agric. Biotechnol. 2024, 103142.

Chatterjee, S.; Barman, S.; Chakraborty, R. Combined effects of ionic liquid and tungsten–halogen radiation on heterogeneous hydrolysis kinetics of waste papaya epidermis for production of total reducing sugar.Waste Biomass Valorization. 2019, 10, 1845-1855.

Somaprabha, A.; Saravanan, K.; Durairaj, K. Evaluation and production of bio-ethanol using agricultural waste with banana Pseudostem and peels of pine apple and banana peel. Int. Res. J. Mod. Eng. Technol. Sci. 2023, 4, 2023-2036.

Sukmaningtyas, R. P. Pretreated of banana pseudo-stem as raw material for enzymatic hydrolysis and bio-ethanol production. In MATEC Web of Conferences (Vol. 154, p. 01035). EDP Sciences. 2018.

Prakash, H.; Chauhan, P. S.; General, T.; Sharma, A. K. Development of eco-friendly process for the production of bio-ethanol from banana peel using inhouse developed cocktail of thermo-alkali-stable depolymerizing enzymes.Bioprocess. Biosyst. Eng. 2018, 41, 1003-1016.

Omonije, O. O.; Chidi, E. E.; Adamu, K. Y.; Olutoye, M. A. Response Surface Optimization for Microwave-Assisted Alkaline Pretreatment of Plantain Pseudostem Biomass for Bio-ethanol Production. Chem Search Journal. 2021, 12, 113-128.

Abril-González, M.; Vele-Salto, A.; Pinos-Vélez, V. Kinetic study of acid hydrolysis of the glucose obtained from banana plant. ChemEngineering. 2023, 7, 39.

Liu, F.; Li, J.; Yu, H.; Li, Y.; Wang, Y.; Gao, H.; Peng, L. Optimizing two green-like biomass pretreatments for maximum bio-ethanol production using banana pseudostem by effectively enhancing cellulose depolymerization and accessibility.Sustainable Energy Fuels. 2021, 5, 3467-3478.

Legodi, L. M.; LaGrange, D. C.; Jansen van Rensburg, E. L.; Ncube, I. Enzymatic hydrolysis and fermentation of banana pseudostem saccharified substance to produce bio-ethanol.Int. J. Microbiol. 2021, 1-14.

Park, W.M.; Park, H.G.; Rhee, SJ.; Kang, K.I.; Lee, C.H.; Yoon, K.E. Property of wine from domestic grape, Vitis labrusca cultivar. Campbell's early, fermented by carbonic maceration vinification process. Korean. J. Food. Sci. Technol. 2004, 36, 773–8.

Islam, M. Z., Asad, M. A., Hossain, M. T., Paul, S. C., & Sujan, S. A. Bioethanol production from banana pseudostem by using separate and cocultures of cellulase enzyme with Saccharomyces cerevisiae. J. Environ. Sci. Technol.2019, 12, 157-163.

Ludwig, T. G.; Goldberg, H. J. The anthrone method for the determination of carbohydrates in foods and in oral rinsing. J. Dent. Res. 1956, 35, 90-94.

Tse, T. J., Wiens, D. J., & Reaney, M. J. (2021). Production of bioethanol—A review of factors affecting ethanol yield. Fermentation, 7(4), 268.

Pinney, M. M., Mokhtari, D. A., Akiva, E., Yabukarski, F., Sanchez, D. M., Liang, R., ... & Herschlag, D. (2021). Parallel molecular mechanisms for enzyme temperature adaptation. Science, 371(6533), eaay2784.

Van Rooyen, R. (2007). Genetic engineering of the yeast Saccharomyces cerevisiae to ferment cellobiose (Doctoral dissertation, Stellenbosch: Stellenbosch University).

Shrotri, A., Kobayashi, H., & Fukuoka, A. (2017). Catalytic conversion of structural carbohydrates and lignin to chemicals. In Advances in catalysis (Vol. 60, pp. 59-123). Academic Press.